Pergamon

Tetrahedron, Vol. 53, No. 18, pp. 6433-6464, 1997

0040-4020/97 $17.00 + 0.00

PII: S0040-4020(97)00302-5

The Tunable Transmission of the Aromatic Character of the Aglycone Through the Anomeric Effect in C-nucleosides Drives its Own Sugar Conformation : A Thermodynamic Study

Ingrid Luyten, Christophe Thibaudeau, Anders Sandström and Jyoti Chattopadhyaya*

Department of Bioorganic Chemistry, Box 581, Biomedical Centre,
University of Uppsala, S-751 23 Uppsala, Sweden

(E-mail: jyoti@bioorgchem.uu.se. Fax: +4618554495]

Abstract: The anomeric and the gauche effects are two competing stereoelectronic forces that drive the North (N) (C2'-exo-C3'-endo) $\rightleftarrows$ South (S) (C2'-endo-C3'-exo) pseudorotational equilibrium in nucleosides (ref 1). The quantitation of the energetics of pD dependent N $\rightleftarrows$ S pseudorotational equilibria of the pentofuranose moiety in C-nucleosides **1 - 7** shows that the strength of the anomeric effect of the constituent heterocyclic moiety at C1' is dependent upon the unique aromatic nature of the nucleobase, which is tuned by the pD of the medium. The force that drives the protonation $\rightleftarrows$ deprotonation equilibrium of the heterocyclic nucleobases in C-nucleosides is transmitted through the anomeric effect to drive the two-state N$\rightleftarrows$ S pseudorotational equilibrium of the constituent furanose (the energy pump), which is supported by the following observations: (i) The enhanced strength ($\Delta\Delta G^{298}{}_{(P\text{-}N)}$) of the anomeric effect in the protonated (P) nucleoside compared to the neutral (N) form is experimentally evidenced by the increased preference of N-type sugar conformation with pseudoaxial nucleobase by 2.0 kJ/mol for formycin B (**1**), 1.4 kJ/mol for formycin A (**2**), 1.4 kJ/mol for 9-deazaadenosine (**3**) and 1.9 kJ/mol for Ψ-isocytidine (**4**). (ii) In contrast, the S-type sugar conformer, which places the nucleobase in pseudoequatorial orientation, is considerably more preferred in the alkaline medium owing to the weakening of the anomeric effect in the N1 deprotonated (D) formycin B, and N3-deprotonated Ψ–isocytidine, Ψ–uridine and 1-methyl-Ψ–uridine compared to the neutral counterparts by $\Delta\Delta G^{\circ}{}_{(N\text{-}D)}$ of 0.2 kJ/mol for formycin B (**1**), 1.6 kJ/mol for Ψ-isocytidine (**4**), 1.7 kJ/mol for Ψ-uridine (**5**), 0.8 kJ/mol for 1-methyl-Ψ-uridine (**6**). (iii) The quantitation of the pD-dependent drive of N $\rightleftarrows$ S pseudorotational equilibria in C-nucleosides **1 - 6** has allowed us to independently measure the pK_a of the constituent heterocyclic nucleobases. (iv) A simple comparison of ΔG^{298}_{N} or ΔG^{298}_{P} or ΔG^{298}_{D} values of all C-nucleosides **1 - 7** (Table 1) with N-nucleosides (ref 1) shows that the C1' substituent promoted anomeric drive of N $\rightleftarrows$ S equilibrium to N-sugar is weaker in C-nucleosides than in N-nucleosides, but their respective flexibilities from the neutral to the protonated or to the deprotonated state is completely aglycone-dependent. © 1997 Elsevier Science Ltd.

The structural characteristic of C-nucleosides, found ubiquitously in various tRNAs[2], is distinguished by carbon-carbon bond linking the ribofuranosyl moiety to a heterocyclic base at the anomeric center. Many of them are antibiotics and exhibit anticancer and/or antiviral activity[3]. The primary structure of a C-nucleoside consists of a purine or a pyrimidine aglycone which is covalently bonded from C9 of purine or C5 of pyrimidine to C1' of a D-ribopentofuranose in a β-configuration. While the aglycone moieties of the N-nucleoside are directly involved in carrying the genetic information and its propagation in the replication machinery by Watson-Crick or Hoogsteen hydrogen bonded base-pairing, very little is known about the stereochemical role of C-nucleosides in biology in general, except for the fact that their presence in certain

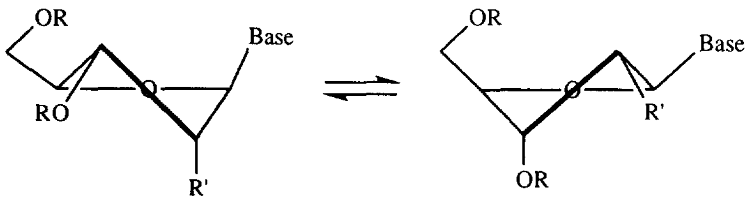

North sugar ($C_{3'}$-*endo*-$C_{2'}$-*exo*)
Phase angle (P) : $0° \leq P \leq 36°$;
Puckering amplitude (Ψ_m) : $30° \leq \Psi_m \leq 46°$

South sugar ($C_{2'}$-*endo*-$C_{3'}$-*exo*)
Phase angle (P) : $144° \leq P \leq 190°$;
Puckering amplitude (Ψ_m) : $30° \leq \Psi_m \leq 46°$

Scheme 1. The dynamic two-state pseudorotational equilibrium of the β-D-pentofuranose moiety is determined by the nature and relative orientations of substituents.

tRNAs is absolutely vital to the biochemical function[2]. In contradistinction to our knowledge on the thermodynamics of the stereoelectronic anomeric[1,4a-d,5-10] and gauche[1,4e-j] effects in N-nucleosides, very little is known about how the C-aglycone and the pentofuranose moiety form the steric and stereoelectronic partnership, or why they are so important for the structural and functional role of tRNAs.

The strength of the anomeric effect in an N- or C-nucleoside can be assessed in a quantitative manner by monitoring the preference of its sugar moiety for N-type (*i.e.* pseudoaxial aglycone) over S-type (*i.e.* pseudoequatorial aglycone) conformation. We have shown by the detailed comparative analysis of temperature-dependent conformational preferences of the two-state N $\rightleftarrows$ S sugar equilibrium (Scheme 1) in a series of 1-deoxy-, 1,2-dideoxy- and 1,2,3-trideoxypentofuranoses with the furanose moieties in adenosine, guanosine, ribothymidine, uridine and cytidine and their 2'-deoxy and 2',3'-dideoxy counterparts that the strength of the anomeric effect in nucleosides is as follows: adenine < guanine < thymine < uracil < cytosine[1a,11]. We found that the N7 or N1 protonation of adenosine or guanosine (or their 2'-deoxy counterparts) enhances the strength of the anomeric effect as evidenced by an increased preference of N-type conformers compared with the situation at neutral pD. On the other hand, N1 or N3 deprotonation of guanosine, uridine or ribothymidine (or of their 2'-deoxy counterparts) leads to an increased proportion of S-type conformers, as a result of the reduction of the strength of the anomeric effect[1n]. These observations clearly showed the followings: (i) The drive of the sugar N $\rightleftarrows$ S pseudorotational equilibria is indeed dictated by the competing anomeric and gauche effects in N-nucleosides. (ii) The strength of the anomeric effect can be tuned by the transmission of the energetics of the protonation $\rightleftarrows$ deprotonation equilibria of the heterocyclic aglycone through the glycosyl-nitrogen, and (iii) the strengths of the gauche effects are controlled by the electronegativity of the substituent. Thus, these works, for the first time, have given a clear rational of how the local structure within a polynucleotide chain is controlled by the actual nucleobase composition. In this regard, the base-base stacking, hydration, steric effects and inter- and intramolecular H-bonding as well as conformational constraints such as those imposed by the ring closure as in the lariat-RNA are important.

Hence, it was of considerable interest to us to determine whether the observed unique pD-dependent transmission of the energetics of the anomeric effect in N-nucleosides is also operative in case of C-nucleosides. We argued that if the anomeric effect really exists in C-nucleosides, just as in N-nucleosides[1n], the change of the electronic character of the purine and pyrimidine bases in C-nucleosides **1** - **7** (either by protonation or by deprotonation) should result in the modulation of its strength, which, in turn, should be transmitted to alter the observable bias of the N $\rightleftarrows$ S pseudorotational equilibria. We here show, by the

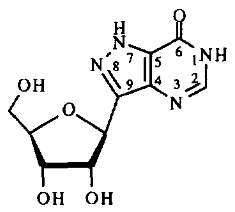

1

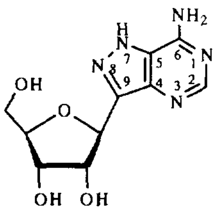

2

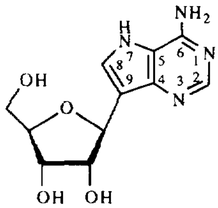

3

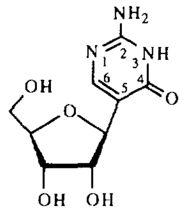

4

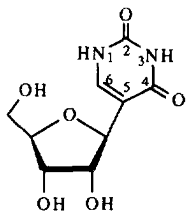

5

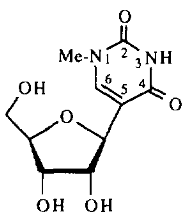

6

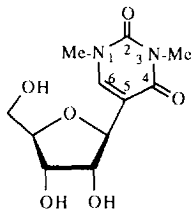

7

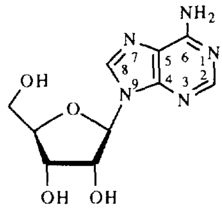

8

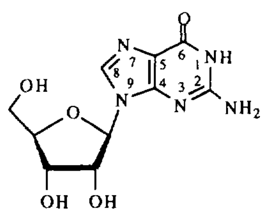

9

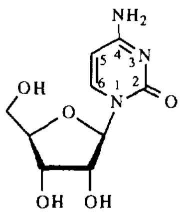

10

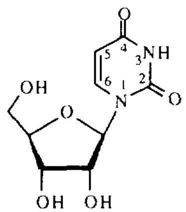

11

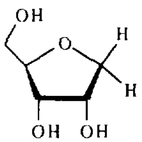

12

quantitation of the energetics of pD-dependent N$\rightleftarrows$ S pseudorotational equilibria of the pentofuranose moiety in **1** - **7**, that (i) the strength of the anomeric effect of each C-nucleoside **1** - **6** is aglycone-dependent and tunable depending upon the pD of the medium, due to the change in the aromatic character of its nucleobase, (ii) the force that drives the protonation$\rightleftarrows$ deprotonation equilibrium of a heterocyclic aglycone in a particular C-nucleoside also drives the two-state N$\rightleftarrows$ S pseudorotational equilibrium of the constituent furanose through the fine tuning of the anomeric effect, and owing to these reasons, (iii) an independent measurement of the pK_a of the constituent nucleobases in C-nucleosides has been possible by quantitation of the pD-dependent energetics of the two-state N $\rightleftarrows$ S pseudorotational equilibria, and (iv) a comparison of $\Delta\Delta G^{298}{}_{(P\text{-}N)}$ and $\Delta\Delta G^{298}{}_{(N\text{-}D)}$ amongst pyrimidine C- and N-nucleosides show that the anomeric tunability is 5-9 times more pronounced in the pyrimidine C-nucleosides, whereas there is no significant difference in the anomeric tunability between purine C- and N-nucleosides.

Results

(I) Method to determine the thermodynamics of the dynamic N $\rightleftarrows$ S pseudorotational equilibria

The vicinal proton-proton coupling constants ($^3J_{HH}$) of formycin B[11] (**1**), formycin A[12] (**2**), 9-deazaadenosine (**3**), Ψ-isocytidine[13] (**4**), Ψ-uridine[13] (**5**), 1-methyl-Ψ-uridine[13] (**6**) and 1,3-dimethyl-Ψ-uridine[13] (**7**) in D_2O solution were measured over a 278 - 358 K temperature range at a wide range of acidic, neutral and alkaline conditions at ~0.5 pD unit intervals (0.5 < pD < 12.0). The data on $^3J_{HH}$ variation at the two extreme temperatures (278 and 358K) and at each pD are shown for all nucleosides **1 - 7** in Tables 2 - 5 in the experimental section.

The temperature-dependent $^3J_{HH}$ in **1 - 7** at various pD values were interpreted in terms of a two-state N $\rightleftarrows$ S conformational equilibrium with the use of the computer program PSEUROT (ver. 5.4)[14,19]. Five parameters are needed to describe the actual state of the N $\rightleftarrows$ S conformational equilibrium (Scheme 1): the phase angles of pseudorotation for N(P_N) and S(P_S) pseudorotamers; the corresponding maximum puckering amplitudes [Ψ_m(N) and Ψ_m(S)]; and the molar fraction of S-type conformers ($x_S = 1 - x_N$). The conformational hyperspace covered by the PSEUROT analyses and the resulting optimized geometries of N and S conformers for all C-nucleosides **1 - 7** at various pDs are described in the experimental section as well as in Tables 6 - 12.

The mole fractions of S-type conformers at several temperatures throughout the 278 - 358 K range (10 K step) at each pD, obtained through several pseudorotational analyses (typically 5000-20000, see experimental section and Tables 6-12), were used in the subsequent van't Hoff type analyses to obtain the slopes and intercepts. The averages of all these slopes and intercepts, shown in Tables 6-12 together with their corresponding standard deviations, were used to calculate the average enthalpy (ΔH°) and the average entropy (ΔS°) and subsequently the free energy values, $\Delta G^{298} = \Delta H° - T\Delta S°$ at 298 K of the N $\rightleftarrows$ S pseudorotational equilibria in **1 - 7** at each pD. The ΔH°, the -TΔS° and the ΔG^{298} values at 298K of N $\rightleftarrows$ S pseudorotational equilibrium in **1 - 7**, as a function of pD, are presented in Tables 6 - 12 together with their corresponding standard deviations, indicated in parentheses. The ΔH°, the -TΔS° and the ΔG^{298} values in Table 1 in the protonated, neutral and deprotonated state of C-nucleosides **1- 7** are obtained by a standard Monte Carlo fitting procedure to the minimum χ^2 value using the program proFit[20]. *The signs of the thermodynamic parameters in Tables 1, 6 - 12 are arbitrarily chosen[1] in such a way that the positive values indicate the drive of N $\rightleftarrows$ S equilibrium to N, whereas the negative values describe the drive toward S.* The subscripts N, P or D denote neutral, protonated or deprotonated state.

Since many steps, each with its own standard deviation (see the error estimation in the experimental section), are involved in obtaining ΔG^{298} through van't Hoff type analysis, we have used a second approach to calculate the ΔG^{298} values. In this approach, we have taken the average of the logarithms of the ratios of mole fractions of S- and N-type conformers at 298K at each pD, indicated as $\ln_{av}(x_S/(1-x_S))$, which corresponds to 2 to 3 % unit error in population of the S-type conformers. The free energy ΔG^{298} can then be directly calculated from the average logarithm, $\ln_{av}(x_S/(1-x_S))$, by using the Gibbs equation $\Delta G^T = -(RT/1000)\ln_{av}(x_S/(1-x_S))$ where $1-x_S = x_N$, R is the gas constant and T is the temperature. The free energies at 298 K, obtained by using the formula $\Delta G^{298} = -R * 0.298 * \ln_{av}(x_S/(1-x_S))$, are presented in the last column of Tables 6-12 with their corresponding standard deviations in parentheses. The comparison of the ΔG^{298} values obtained through the two above described procedures shows that their values are very similar, but their corresponding standard deviations are different. The second approach shows a smaller error because it does not involve any linear regression analysis to obtain ΔG^{298}. Throughout this paper, we have used the ΔG^{298} values obtained by the second approach. In this work, ΔG^{298} term has been employed to quantify the total anomeric drive of the sugar conformation, which is the result of intrinsic stereoelectronic and steric component of the aglycone (*i.e.* ΔH° term), whereas ΔS° value represents the entropy of the system.

(II) The thermodynamics of pD-dependent N $\rightleftarrows$ S pseudorotational equilibria of C-nucleosides

We have earlier shown that the specific nature of glycosyl nitrogen in N-ribonucleosides **8** - **11** controls N $\rightleftarrows$ S pseudorotational equilibria of the sugar moieties both by the distinct anomeric effect and the competing gauche effect of [N-C1'-C2'-O2'] fragment[1a-n] We have also shown earlier that in ribonucleosides the strength of gauche effect in [$N_{(purine)}$-C1'-C2'-O2'] and [$N_{(pyrimidine)}$-C1'-C2'-O2'] fragments, which both drive the pseudorotational equilibrium towards S-type conformations are different[1a-n]. It has been demonstrated by us that protonation or deprotonation of a particular heterocyclic N-nucleobase in **8** - **11** reinforce or weaken the strength of the intrinsic anomeric and [N-C1'-C2'-O2'] gauche effects because of the change of electronic character of the glycosyl nitrogen. The differences observed in ΔH°, ΔS° and ΔG^{298} values of the N $\rightleftarrows$ S equilibria in **8** - **11** at different pD values (see Table 1 and ref. 1n) reflect the combined changes in the drive towards the N-type conformers by the anomeric effect and towards the S-type by the [N-C1'-C2'-O2'] gauche effect.

In C-nucleosides, there is no [N-C1'-C2'-O2'] gauche effect for obvious reasons. Hence, the drive of the N $\rightleftarrows$ S pseudorotational equilibria by a particular heterocyclic nucleobase in C-nucleosides **1** - **7** at the neutral, protonated or deprotonated state results only from the modulation of the strength of the anomeric effect. Thus, the differences observed in ΔH°, ΔS° and ΔG^{298} values of the N $\rightleftarrows$ S equilibria in C-nucleosides **1** - **7** at different pDs (Tables 6-12) reflect the change of the protonation $\rightleftarrows$ deprotonation equilibria, that tune the electronic nature of the C-aglycone and consequently the strength of its anomeric effect, which, in turn, is transmitted to dictate the ΔG° of the two-state N $\rightleftarrows$ S sugar equilibrium (the energy pump)[1n].

(a) The energetics of N $\rightleftarrows$ S equilibria of the neutral C-nucleosides

The values of enthalpy (ΔH°_{N}), entropy contribution ($-T\Delta S^{\circ}_{N}$) and free-energy (ΔG°_{N}) of N $\rightleftarrows$ S equilibria as well as populations of S-type sugars at 298K ($\%S^{298}_{N}$) in the neutral states of **1** - **7** are given in Table 1. In the neutral states ΔH°_{N} values predominate in the drive of the N $\rightleftarrows$ S equilibrium of formycin B (**1**), formycin A (**2**), 9-deazaadenosine (**3**) and Ψ-isocytidine (**4**) towards S-type conformations over the weaker entropy contributions ($-T\Delta S^{\circ}_{N}$) which oppose ΔH°_{N} term by favoring N-type (Table 1). In the case of Ψ-uridine (**5**), 1-methyl-Ψ-uridine (**6**) and 1,3-dimethyl-Ψ-uridine (**7**) ΔH°_{N} and $-T\Delta S^{\circ}_{N}$ contributions are of comparable strength (Table 1), and they oppose each other. As a result, the N $\rightleftarrows$ S pseudorotational equilibria in all C-nucleosides **1** - **7** are controlled by negative ΔG^{298}_{N} values which correspond to 53 - 88 % S at 298 K (Table 1).

(b) The energetics of N ⇄ S equilibria of the protonated C-nucleosides

As the acidity of the solution increases, a shift of the N ⇄ S equilibria of **1** - **4** to more N-type conformation (Tables 6 - 9) (*i.e.* pseudoaxial aglycone) is observed until the complete protonation of the constituent heterocycle is achieved, as evident by the plateau of the N ⇄ S equilibria (Table 1 and Figs 1 - 7).

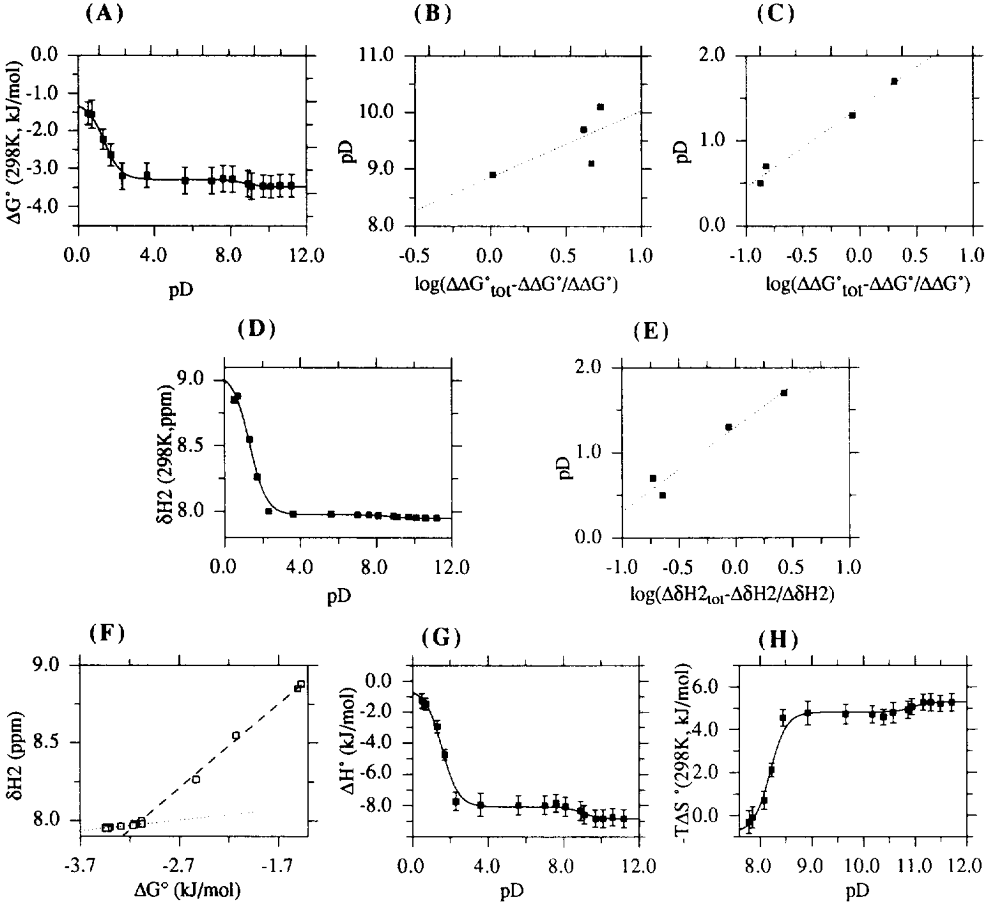

Figure 1. (A) The plot of experimental ΔG^{298} values (from second approach, see text) for the N ⇄ S pseudorotational equilibrium of formycin B (**1**) as a function of pD (Table 6). The sigmoidal curve is the best iterative least-squares fit of the 16 pD-dependent experimental ΔG^{298} values for formycin B (**1**) and these data are used in the Hill plots presented in panel B and C to determine the pK_a values of the aglycone (see experimental section). **(B)** The straight line (R=0.868) has a slope of 0.8 (σ = 0.4) and pK_a of 9.1 (σ = 0.2). **(C)** The straight line (R=0.980) has a slope of 1.0 (σ = 0.1) and pK_a of 1.4 (σ = 0.1). **(D)** The plot of pD-dependent ^{1}H chemical shifts at 298K of H2 for formycin B (**1**), showing a sigmoidal curve which is the best iterative least-squares fit of the 16 pD-dependent experimental chemical shifts for formycin B (**1**). These data are used in the Hill plot presented in panel E to determine independently the pK_a value of the aglycone (see experimental section). **(E)** The straight line (R=0.975) has a slope of 1.0 (σ = 0.1) and pK_a of 1.3 (σ = 0.1). **(F)** Plots of the correlation of the pD-dependent ^{1}H chemical shifts at 298K as a function of pD-dependent ΔG^{298} for the N ⇄ S pseudorotational equilibrium of formycin B (**1**) showing straight lines. The line (----), showing the correlation from pD=0.5 to 7.6, has a correlation coefficient of 0.914, a slope of 0.07 (σ = 0.01) and an intercept of 8.20 (σ = 0.04). The line (....), showing the correlation from pD=7.6 to 11.2, has a correlation coefficient of 0.997 a slope of 0.54 (σ = 0.01) and an intercept of 9.72 (σ = 0.03). **(G)** The plot of experimental ΔH° values for the N ⇄ S pseudorotational equilibrium of formycin B (**1**) as a function of pD (Table 6). The sigmoidal curve is the best iterative least-squares fit of the 16 pD-dependent experimental ΔH° values

Table 1. Thermodynamic data of the N $\rightleftarrows$ S pseudorotational equilibria of the β-D-ribofuranose moiety in **1** - **12** with fully protonated, neutral and fully deprotonated nucleobases[a] and the corresponding pK_a values.

	The energetics of N $\rightleftarrows$ S equilibrium with fully protonated nucleobase [a]						The energetics of N $\rightleftarrows$ S equilibrium with neutral nucleobase[a]						The energetics of N $\rightleftarrows$ S equilibrium with fully deprotonated nucleobase [a]				
	ΔH°_P	ΔS°_P	$-T\Delta S^\circ_P$	ΔG^{298}_P	$\%S^{298}_P$	$pK_a{}^b$	ΔH°_N	ΔS°_N	$-T\Delta S^\circ_N$	ΔG^{298}_N	$\%S^{298}_N$	$pK_a{}^c$	ΔH°_D	ΔS°_D	$-T\Delta S^\circ_D$	ΔG^{298}_D	$\%S^{298}_D$
(1)	-0.5 (0.1)	2.7 (0.3)	-0.8 (0.1)	-1.3 (0.1)	63	1.4 (1.3)	-8.1 (0.1)	-16.1 (0.3)	4.8 (0.1)	-3.3 (0.1)	79	8.9 (8.8)	-8.8 (0.1)	-17.8 (0.3)	5.3 (0.1)	-3.5 (0.1)	80
(2)	-2.4 (0.1)	-1.3 (0.3)	0.4 (0.1)	-2.0 (0.1)	69	4.5 (4.4)	-8.1 (0.5)	-15.8 (1.3)	4.7 (0.4)	-3.4 (0.1)	80	- (9.5)	-8.1 (0.5)	-15.8 (1.3)	4.7 (0.4)	-3.4 (0.1)	80
(3)	-7.4 (0.2)	-12.4 (1.0)	3.7 (0.3)	-3.6 (0.1)	81	5.9 (6.0)	-14.2 (0.4)	-30.5 (1.3)	9.1 (0.4)	-5.0 (0.1)	88	-	-	-	-	-	-
(4)	4.2 (0.1)	12.8 (0.6)	-3.8 (0.2)	0.5 (0.1)	45	3.6 (3.6)	-1.9 (0.1)	-2.0 (0.3)	0.6 (0.1)	-1.4 (0.1)	63	9.2 (9.0)	-7.9 (0.2)	-16.4 (0.6)	4.9 (0.2)	-3.0 (0.1)	77
(5)	-	-	-	-	-	-	0.7 (0.2)	4.7 (0.6)	-1.4 (0.2)	-0.6 (0.1)	57	9.4 (9.1)	-4.5 (0.1)	-7.4 (0.3)	2.2 (0.1)	-2.3 (0.1)	72
(6)	-	-	-	-	-	-	1.6 (0.1)	6.0 (0.3)	-1.8 (0.1)	-0.7 (0.1)	57	9.9 (9.7)	-3.0 (0.1)	-5.1 (0.3)	1.5 (0.1)	-1.5 (0.1)	64
(7)	-	-	-	-	-	-	2.0 (0.1)	7.7 (0.3)	-2.3 (0.1)	-0.3 (0.1)	53						
(8)	-0.2 (0.1)	1.3 (0.6)	-0.4	-0.5	55	3.5 (3.5)	-4.4 (0.2)	-8.7 (0.5)	2.6	-1.8	67	-	-	-	-	-	-
(9)	5.4 (0.2)	14.0 (1.7)	-4.2	1.5	35	2.1 (2.1)	-3.3 (0.2)	-6.2 (0.7)	1.8	-1.5	65	9.6 (9.4)	-7.6 (0.5)	-16.1 (0.8)	4.8	-2.8	76
(10)	5.2 (0.2)	11.1 (1.3)	-3.3	1.9	32	4.0 (4.1)	2.3 (0.1)	2.8 (1.6)	-0.8	1.5	35	-	-	-	-	-	-
(11)	-		-	-	-	-	-2.0 (0.2)	5.6 (0.9)	1.7	0.3	47	9.6 (9.4)	0.3 (0.1)	0.7 (1.1)	-0.2	0.1	49
(12)							0.4 (1.1)	-5.1 (3.5)	1.5	1.9							

(**1**) formycin A, (**2**) formycin B, (**3**) 9-deazaadenosine, (**4**) Ψ-isocytidine, (**5**) Ψ-uridine, (**6**) 1-methyl-Ψ-uridine, (**7**) 1,3-dimethyl-Ψ-uridine, (**8**) adenosine, (**9**) guanosine, (**10**) cytidine, (**11**) uridine and (**12**) 1-deoxy-D-ribofuranose. [a] The ΔH°, -TΔS° (at 298 K) and $\Delta G^{298}$are in kJ/mol. The standard deviations (σ) are in parentheses. The subscripts 'N', 'P' and 'D' denotes respectively the neutral, the protonated state and the deprotonated states. The plateaus in the acidic, neutral and alkaline ranges for ΔH°, ΔS° and ΔG^{298}values were obtained by the iterative nonlinear least-square fitting procedure of the experimental ΔH°, ΔS° (not shown) and ΔG^{298} values (Figs. 1 - 7 for **1** - **7**, for **8** - **11**, data are taken from ref. 1n) at several pDs (Tables 6 - 12 for ΔH°, -TΔS° and ΔG^{298} at various pDs for **1** - **7**, for **8** - **11**, data are taken from ref. 1n). [b]The pK_a of the fully protonated nucleobase. [c]The pK_a of the neutral base. The pK_a were calculated through the Hill plots of pD as a function of $\log(\Delta\Delta G^{298}_{tot} - \Delta\Delta G^{298}/\Delta\Delta G^{298})$ (Fig. 1 - 7). $\Delta\Delta G^{298}_{tot}$ is a total change in ΔG^{298} values between the neutral and the (de)protonated state, whereas $\Delta\Delta G^{298}$is the change in ΔG^{298} value at a given pD relative to the reference neutral state. The pK_a values were also independently calculated through the Hill plots of pD as a function of log(ΔδH(aromatic proton)$_{tot}$ - ΔδH(aromatic proton)/ΔδH(aromatic proton)) (Figs. 1 - 7 for **1** - **7**, for **8** - **11**, data are taken from ref. 1n)). ΔδH(aromatic proton)$_{tot}$ is a total change in chemical shift of the aromatic proton between the neutral and the (de)protonated state, whereas ΔδH(aromatic proton) is the change in chemical shift of the aromatic proton at a given pD relative to the reference neutral state. For Ψ -uridine (**5**), the chemical shift of the anomeric proton was used instead of the chemical shift of the aromatic proton. These pK_a values are in parentheses.

for formycin B (1). **(H)** The plot of experimental -TΔS° values for the N $\rightleftarrows$ S pseudorotational equilibrium of formycin B (1) as a function of pD (Table 6). The sigmoidal curve is the best iterative least-squares fit of the 16 pD-dependent experimental -TΔS°values for formycin B (1).

In the fully protonated state, the N$\rightleftarrows$ S pseudorotational equilibria of formycin B (**1**), formycin A (**2**) and 9-deazaadenosine (**3**) are characterized by less negative ΔG^{298}_{P} values in comparison with the corresponding ΔG^{298}_{N} (Table 1), but for Ψ-isocytidine (**4**) the ΔG^{298}_{P} value is even positive compared with its ΔG^{298}_{N}. This

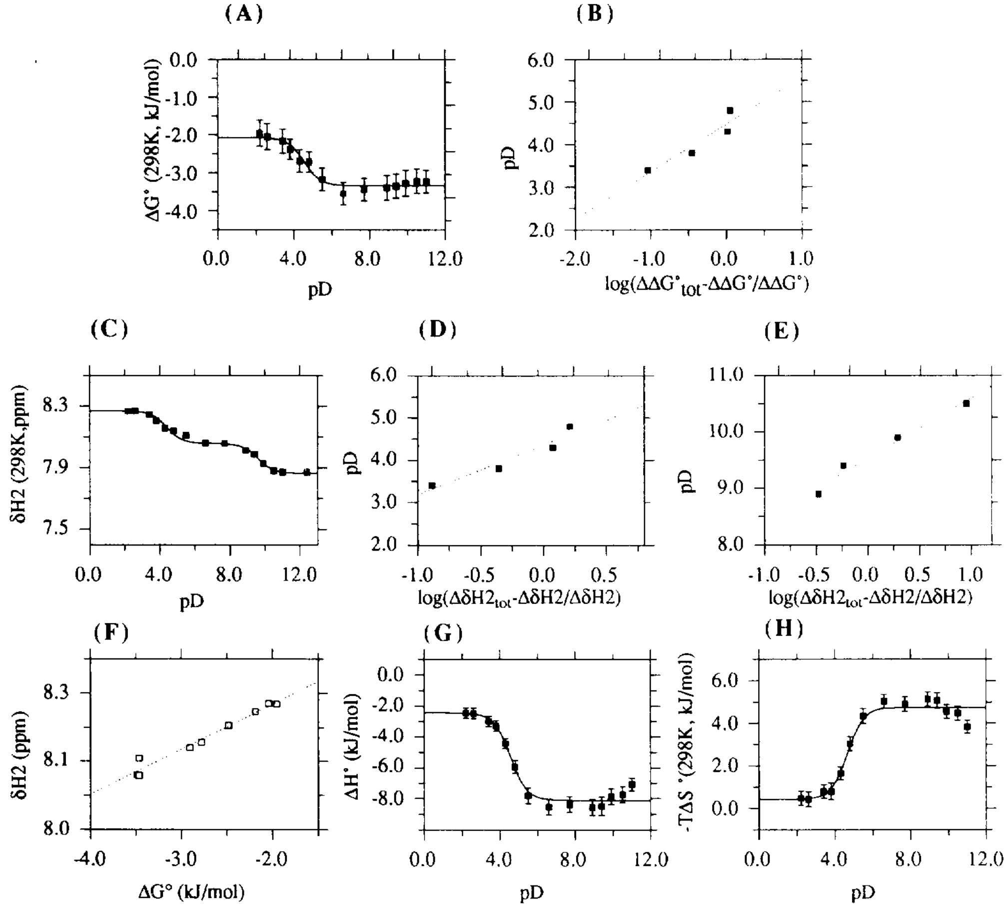

Figure 2. **(A)** The plot of experimental ΔG^{298} values (from second approach, see text) for the N $\rightleftarrows$ S pseudorotational equilibrium of formycin A (2) as a function of pD (Table 7). The sigmoidal curve is the best iterative least-squares fit of the 14 pD-dependent experimental ΔG^{298} values for formycin A (2) and these data are used in the Hill plot presented in panel B to determine the pK_a value of the aglycone (see experimental section). **(B)** The straight line (R=0.985) has a slope of 1.1 (σ = 0.3) and pK_a of 4.5 (σ = 0.2). **(C)** The plot of pD-dependent ^{1}H chemical shifts at 298K of H2 for formycin A (2), showing a sigmoidal curve which is the best iterative least-squares fit of the 14 pD-dependent experimental chemical shifts for formycin A (2). These data are used in the Hill plots presented in panel D and panel E to determine independently the pK_a values of the aglycone (see experimental section). **(D)** The straight line (R=0.961) has a slope of 1.2 (σ = 0.2) and pK_a of 4.4 (σ = 0.1). **(E)** The straight line (R=0.987) has a slope of 1.1 (σ = 0.1) and pK_a of 9.5 (σ = 0.1). **(F)** Plot of the correlation of the pD-dependent ^{1}H chemical shifts at 298K as a function of pD-dependent ΔG^{298} for the N $\rightleftarrows$ S pseudorotational equilibrium of formycin A (2) showing a straight line with a correlation coefficient of 0.983, a slope of 0.13 (σ = 0.01) and an intercept of 8.63 (σ = 0.03). **(G)** The plot of experimental ΔH° values for the

N ⇄ S pseudorotational equilibrium of formycin A (2) as a function of pD (Table 7). The sigmoidal curve is the best iterative least-squares fit of the 14 pD-dependent experimental ΔH° values for formycin A (2). **(H)** The plot of experimental -TΔS° values for the N ⇄ S pseudorotational equilibrium of formycin A (2) as a function of pD (Table 7). The sigmoidal curve is the best iterative least-squares fit of the 14 pD-dependent experimental -TΔS°values for formycin A (2).

indicates a preference for N-type conformer (Table 1) in the protonated state. For formycin B (**1**) the ΔH°_P and the $-T\Delta S^\circ_P$ contributions are comparable and act in a cooperative manner. The negative ΔH°_P values in the fully protonated states drive the N ⇄ S equilibrium in formycin A (**2**) and 9-deazaadenosine (**3**) still towards S-type

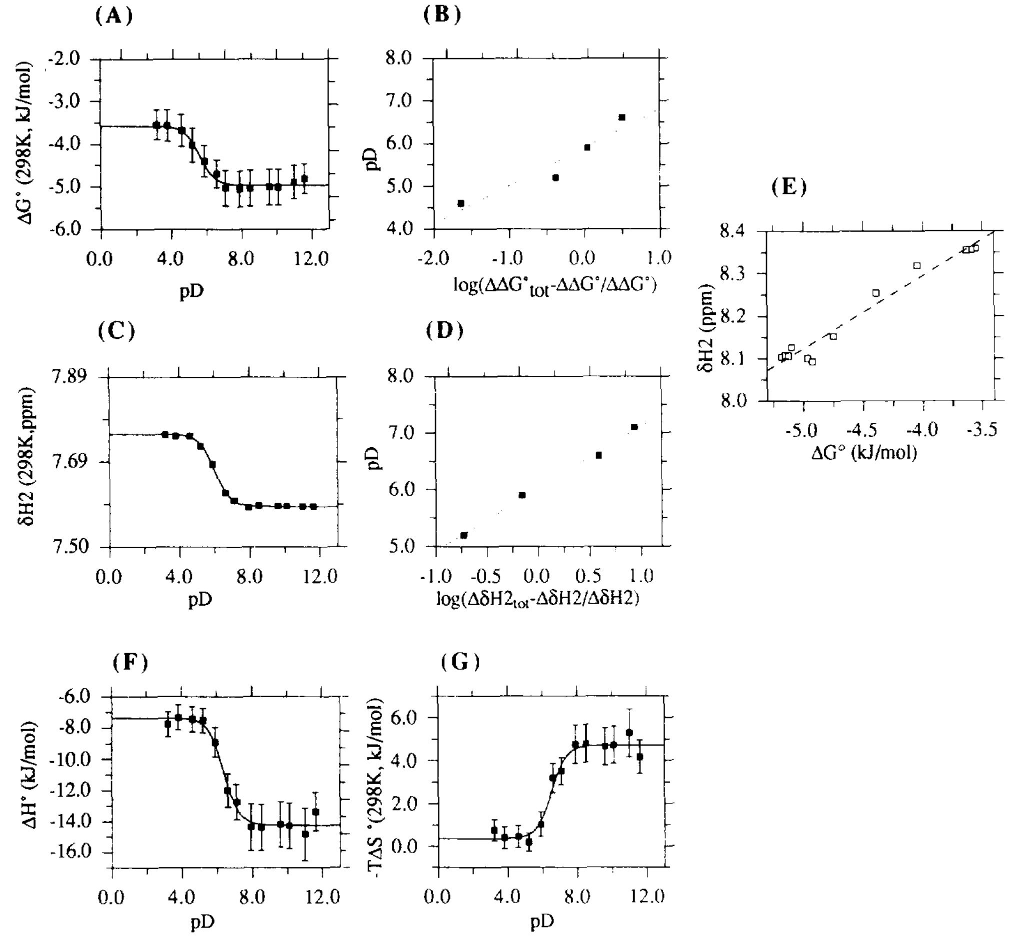

Figure 3. **(A)** The plot of experimental ΔG^{298} values (from second approach, see text) for the N ⇄ S pseudorotational equilibrium of 9-deazaadenosine (3) as a function of pD (Table 8). The sigmoidal curve is the best iterative least-squares fit of the 13 pD-dependent experimental ΔG^{298} values for 9-deazaadenosine (3) and these data are used in the Hill plot presented in panel B to determine the pK_a value of the aglycone (see experimental section). **(B)** The straight line (R=0.950) has a slope of 0.9 (σ = 0.2) and pK_a of 5.9 (σ = 0.2). **(C)** The plot of pD-dependent ^1H chemical shifts at 298K of H2 for 9-deazaadenosine (3), showing a sigmoidal curve which is the best iterative least-squares fit of the 13 pD-dependent experimental chemical shifts for 9-deazaadenosine (3). These data are used in the Hill plots presented in panel D to determine independently the pK_a value of the aglycone (see experimental section). **(D)** The straight line (R=0.997) has a slope of 1.1 (σ = 0.1) and pK_a of 6.0 (σ = 0.1). **(E)** Plot of the correlation of the pD-dependent ^1H chemical shifts at 298K as a function of pD-dependent ΔG^{298} for the N ⇄ S pseudorotational equilibrium of 9-deazaadenosine (3) showing a straight line with a correlation coefficient of 0.982, a slope of 0.17 (σ = 0.01) and an intercept of 8.98 (σ = 0.05). **(F)** The plot of experimental ΔH° values for the N ⇄ S pseudorotational equilibrium of

9-deazaadenosine (3) as a function of pD (Table 8). The sigmoidal curve is the best iterative least-squares fit of the 13 pD-dependent experimental $\Delta H°$ values for 9-deazaadenosine (3). **(G)** The plot of experimental $-T\Delta S°$ values for the N $\rightleftarrows$ S pseudorotational equilibrium of 9-deazaadenosine (3) as a function of pD (Table 8). The sigmoidal curve is the best iterative least-squares fit of the 13 pD-dependent experimental $-T\Delta S°$ values for 9-deazaadenosine (3).

conformations and predominate over the weaker and counteracting $-T\Delta S°_P$ (Table1). For Ψ-isocytidine (4) the positive $\Delta H°_P$ value in the fully protonated state drives the sugar towards N-type conformation, and the

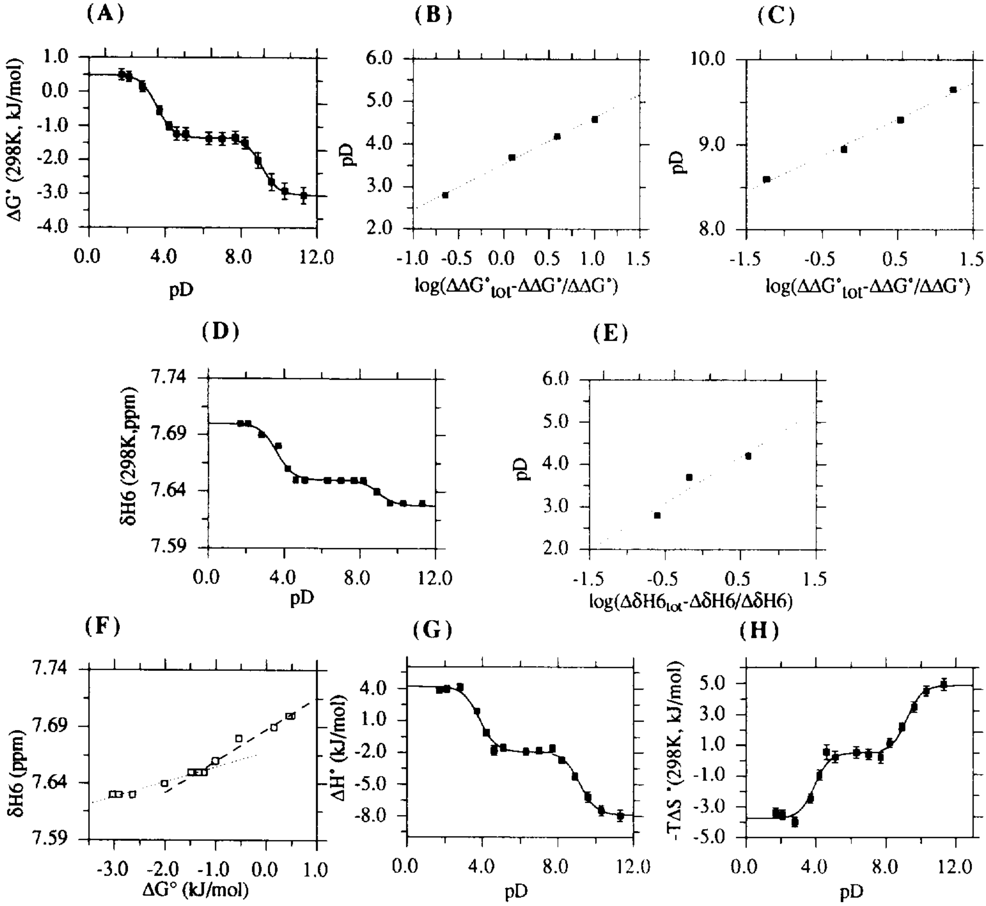

Figure 4. **(A)** The plot of experimental ΔG^{298} values for the N $\rightleftarrows$ S pseudorotational equilibrium of Ψ-isocytidine (4) as a function of pD (Table 9). The sigmoidal curve is the best iterative least-squares fit of the 15 pD-dependent experimental ΔG^{298} values for Ψ-isocytidine (4) and these data are used in the Hill plots presented in panel B and C to determine the pK_a values of the aglycone (see experimental section). **(B)** The straight line (R=0.998) has a slope of 1.1 (σ = 0.5) and pK_a of 3.6 (σ = 0.1). **(C)** The straight line (R=0.996) has a slope of 0.9 (σ = 0.1) and pK_a of 9.2 (σ = 0.1). **(D)** The plot of pD-dependent ^1H chemical shifts at 298K of H6 for Ψ-isocytidine (4) , showing a sigmoidal curve which is the best iterative least-squares fit of the 15 pD-dependent experimental chemical shifts for Ψ-isocytidine (4). These data are used in the Hill plot presented in panel E to determine independently the pK_a value of the aglycone (see experimental section). **(E)** The straight line (R=0.946) has a slope of 1.1 (σ = 0.4 and pK_a of 3.6 (σ = 0.2). **(F)** Plots of the correlation of the pD-dependent ^1H chemical shifts at 298K as a function of pD-dependent ΔG^{298} for the N $\rightleftarrows$ S pseudorotational equilibrium of Ψ-isocytidine (4) showing straight lines. The line (----), showing the correlation from pD=2.1 to 7.7, has a correlation coefficient of 0.990 a slope of 0.03 (σ = 0.01) and an intercept of 7.70 (σ = 0.01). The line (....), showing the correlation from pD=7.7 to 11.3, has a correlation coefficient of 0.969 a slope of 0.01 (σ = 0.01) and an intercept of 7.68 (σ = 0.01).

(G) The plot of experimental ΔH° values for the N ⇄ S pseudorotational equilibrium of Ψ-isocytidine (4) as a function of pD (Table 9). The sigmoidal curve is the best iterative least-squares fit of the 15 pD-dependent experimental ΔH° values for Ψ-isocytidine (4) **(H)** The plot of experimental -TΔS° values for the N ⇄ S pseudorotational equilibrium of Ψ-isocytidine (4) as a function of pD (Table 9). The sigmoidal curve is the best iterative least-squares fit of the 15 pD-dependent experimental -TΔS°values for Ψ-isocytidine (4).

opposing $-T\Delta S^{\circ}_{P}$ is of comparable strength. The shift towards more N-type conformations in **1** - **4** upon complete protonation signifies overall tunability of the strength of the anomeric effect as the protonated

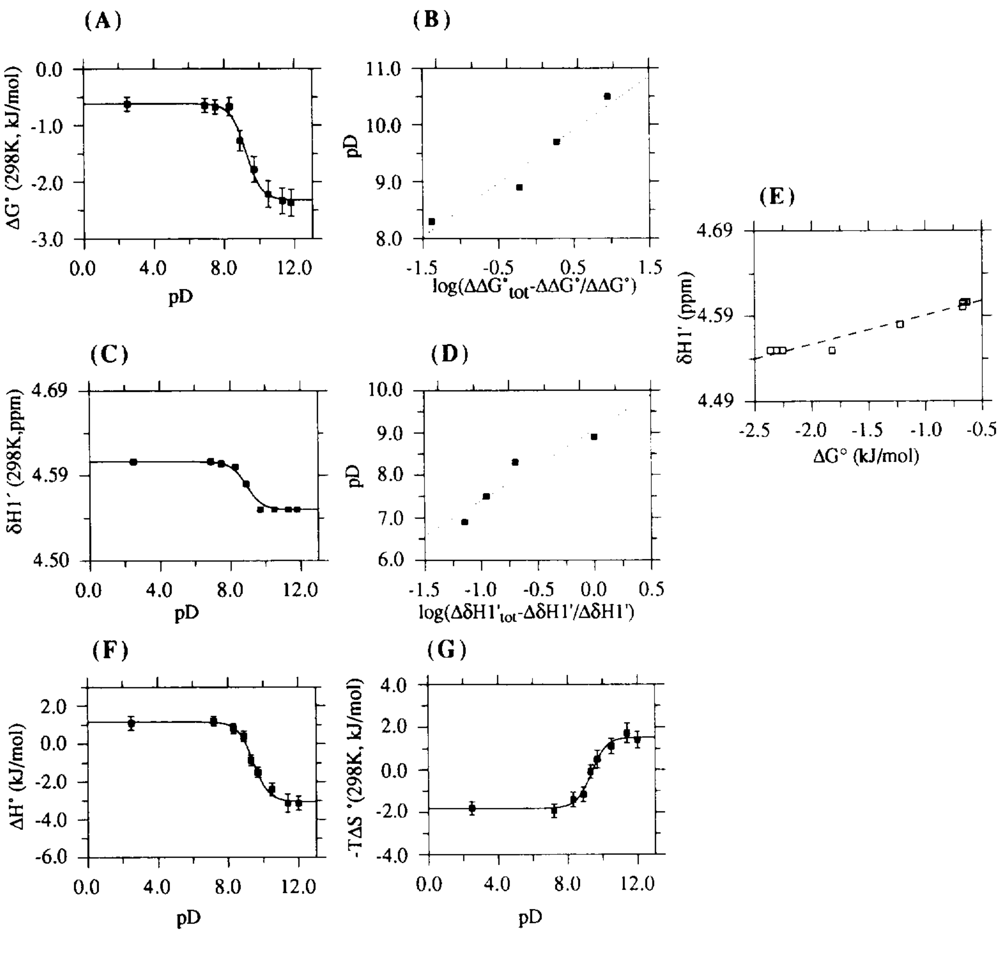

Figure 5. **(A)** The plot of experimental ΔG^{298} values for the N ⇄ S pseudorotational equilibrium of Ψ-uridine (5) as a function of pD (Table 10). The sigmoidal curve is the best iterative least-squares fit of the 9 pD-dependent experimental ΔG^{298} values for Ψ-uridine (5) and these data are used in the Hill plot presented in panel B to determine the pK_a value of the aglycone (see experimental section). **(B)** The straight line (R=0.970) has a slope of 0.9 (σ = 0.2) and pK_a of 9.4 (σ = 0.1). **(C)** The plot of pD-dependent ^1H chemical shifts at 298K of H1' for Ψ-uridine (5), showing a sigmoidal curve which is the best iterative least-squares fit of the nine pD-dependent experimental chemical shifts for Ψ-uridine (5). These data are used in the Hill plots presented in panel D to determine independently the pK_a value of the aglycone (see experimental section). **(D)** The straight line (R=0.944) has a slope of 1.6 (σ = 0.4) and pK_a of 9.1 (σ = 0.3). **(E)** Plot of the correlation of the pD-dependent ^1H chemical shifts at 298K as a function of pD-dependent ΔG^{298} for the N⇄ S pseudorotational equilibrium of Ψ-uridine (5) showing a straight line with a correlation coefficient of 0.978, a

slope of 0.03 (σ = 0.01) and an intercept of 4.63 (σ = 0.01). **(F)** The plot of experimental $\Delta H°$ values for the N $\rightleftarrows$ S pseudorotational equilibrium of Ψ-uridine (**5**) as a function of pD (Table 10). The sigmoidal curve is the best iterative least-squares fit of the 9 pD-dependent experimental $\Delta H°$ values for Ψ-uridine (**5**). **(G)** The plot of experimental $-T\Delta S°$ values for the N $\rightleftarrows$ S pseudorotational equilibrium of Ψ-uridine (**5**) as a function of pD (Table 10). The sigmoidal curve is the best iterative least-squares fit of the 9 pD-dependent experimental $-T\Delta S°$ values for Ψ-uridine (**5**).

aglycone takes up more pseudoaxial orientation, which can be quantified by the subtraction of ΔG^{298}_{N} from ΔG^{298}_{P} (*i.e.* $\Delta\Delta G^{298}_{(P-N)}$). This shows that, from the neutral to the protonated state, the preference for the pseudoaxially oriented aglycone in the N-type sugar has increased by 2.0 kJ/mol for formycin B (**1**), 1.4 kJ/mol for formycin A (**2**), 1.4 kJ/mol for 9-deazaadenosine (**3**) and 1.9 kJ/mol for Ψ-isocytidine (**4**).

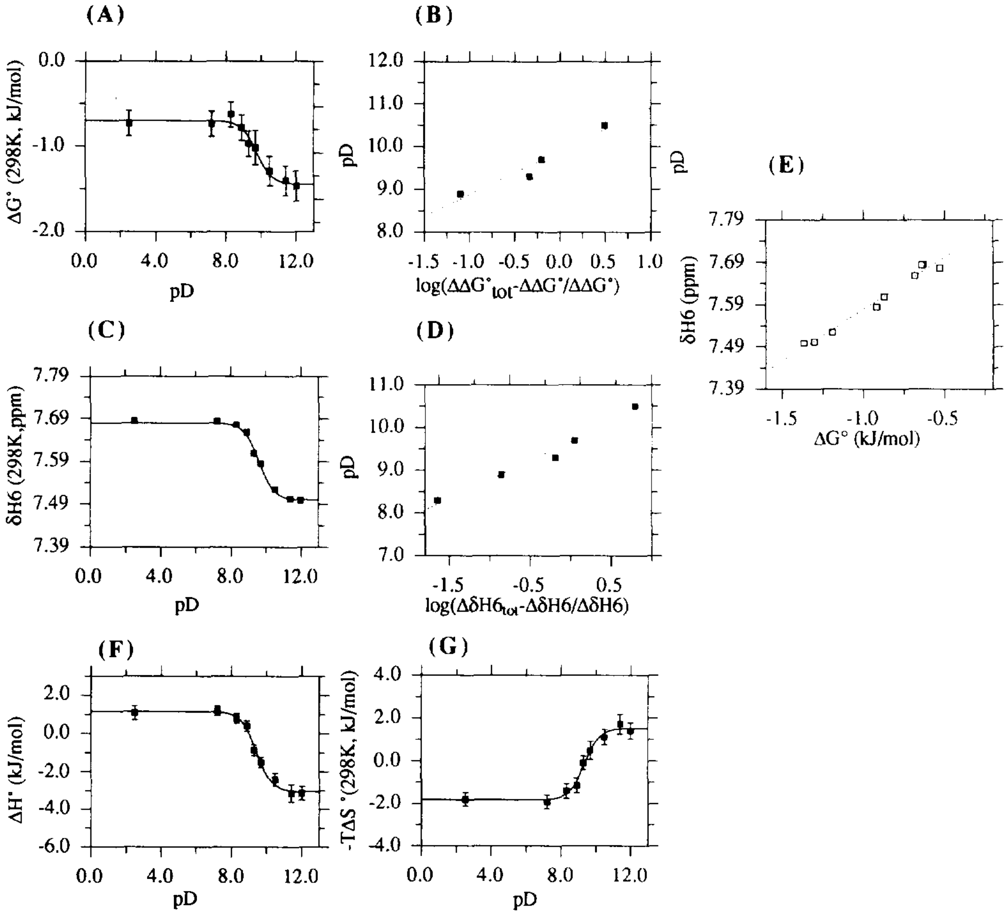

Figure 6 **(A)** The plot of experimental ΔG^{298} values for the N $\rightleftarrows$ S pseudorotational equilibrium of 1-methyl-Ψ-uridine (**6**) as a function of pD (Table 11). The sigmoidal curve is the best iterative least-squares fit of the 9 pD-dependent experimental ΔG^{298} values for 1-methyl-Ψ-uridine (**6**) and these data are used in the Hill plot presented in panel B to determine the pK_a value of the aglycone (see experimental section). **(B)** The straight line (R=0.968) has a slope of 1.0 (σ = 0.2) and pK_a of 9.9 (σ = 0.1). **(C)** The plot of pD-dependent ^1H chemical shifts at 298K of H6 for 1-methyl-Ψ-uridine (**6**), showing a sigmoidal curve which is the best iterative least-squares fit of the nine pD-dependent experimental chemical shifts for 1-methyl-Ψ-uridine (**6**). These data are used in the Hill plots presented in panel D to determine independently the pK_a value of the aglycone (see experimental section). **(D)** The straight line (R=0.988) has a slope of 0.9 (σ = 0.1) and pK_a of 9.7 (σ = 0.1). **(E)** Plot of the correlation of the pD-dependent ^1H chemical shifts at

298K as a function of pD-dependent ΔG^{298} for the N $\rightleftarrows$ S pseudorotational equilibrium of 1-methyl-Ψ-uridine (**6**) showing a straight line with a correlation coefficient of 0.987, a slope of 0.24 (σ = 0.01) and an intercept of 7.86 (σ = 0.02). **(F)** The plot of experimental $\Delta H°$ values for the N $\rightleftarrows$ S pseudorotational equilibrium of 1-methyl-Ψ-uridine (**6**) as a function of pD (Table 11). The sigmoidal curve is the best iterative least-squares fit of the 9 pD-dependent experimental $\Delta H°$ values for 1-methyl-Ψ-uridine (**6**). **(G)** The plot of experimental $-T\Delta S°$ values for the N $\rightleftarrows$ S pseudorotational equilibrium of 1-methyl-Ψ-uridine (**6**) as a function of pD (Table 11). The sigmoidal curve is the best iterative least-squares fit of the 9 pD-dependent experimental $-T\Delta S°$values for 1-methyl-Ψ-uridine (**6**).

(c) The energetics of N $\rightleftarrows$ S equilibria of the deprotonated C-nucleosides

Upon deprotonation, the N $\rightleftarrows$ S equilibria in formycin B (**1**), Ψ-isocytidine (**4**), Ψ-uridine (**5**), 1-methyl-Ψ-uridine (**6**) are shifted towards S-type conformations (*i.e.* pseudoequatorial aglycone), which is reflected in the decrease of $\Delta H°$ and ΔG^{298} values (Tables 6, 9 - 11). The negative $\Delta H°_D$ in the fully deprotonated state drive the N $\rightleftarrows$ S equilibrium in all cases towards S-type conformations and predominates over the weaker opposing $-T\Delta S°_D$ contributions (Table 1). The subtraction of (ΔG^{298}_D) from the corresponding values in the

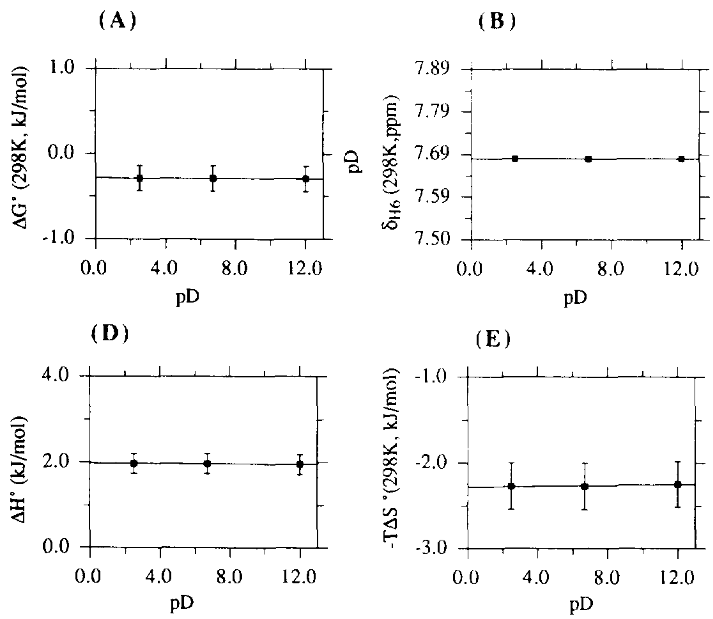

Figure 7 **(A)** The plot of experimental ΔG^{298} values for the N $\rightleftarrows$ S pseudorotational equilibrium of 1,3-dimethyl-Ψ-uridine (**7**) as a function of pD (Table 12). **(B)** The plot of ^1H chemical shifts at 298K of H6 for 1,3-dimethyl-Ψ-uridine (**7**) as a function of pD. **(C)** The plot of experimental $\Delta H°$ values for the N $\rightleftarrows$ S pseudorotational equilibrium of 1,3-dimethyl-Ψ-uridine (**7**) as a function of pD (Table 12). **(D)** The plot of experimental $-T\Delta S°$ values for the N $\rightleftarrows$ S pseudorotational equilibrium of 1,3-dimethyl-Ψ-uridine (**7**) as a function of pD (Table 12).

neutral state (ΔG^{298}_N) (*i.e* $\Delta\Delta G°_{(ND)}$) shows that the energetic preference for the pseudoaxial orientation of the aglycone (as evident by the decrease of N-type conformer population) has weakened by 0.2 kJ/mol for formycin B (**1**), 1.6 kJ/mol for Ψ-isocytidine (**4**), 1.7 kJ/mol for Ψ-uridine (**5**) and 0.8 kJ/mol for 1-methyl-Ψ-uridine (**6**).

(d) The energetics of the tunability of the drive of $N \rightleftarrows S$ equilibrium is C-aglycone dependent

(i) The tunability of the anomeric effect promoted drive of N $\rightleftarrows$ S equilibrium from the neutral to the protonated or to the deprotonated state, *i.e.* $\Delta\Delta G^{298}{}_{(P\text{-}N)}$ or $\Delta\Delta G^{298}{}_{(N\text{-}D)}$, is experimentally evidenced by the increased preference of N-type sugar with pseudoaxial aglycone orientation or S-type with pseudoequatorial aglycone, respectively. Thus, $\Delta\Delta G^{298}{}_{(P\text{-}N)}$ is 2.0 kJ/mol for formycin B (**1**), 1.4 kJ/mol for formycin A (**2**) and 1.4 kJ/mol for 9-deazaadenosine (**3**), which is comparable with those of adenosine (1.3 kJ/mol) and guanosine (3.0 kJ/mol). This means that the anomeric tunability of the C- and N-purines are quite comparable. The only exception we have found so far is for $\Delta\Delta G^{298}{}_{(N\text{-}D)}$ for formycin B (**1**) (0.2 kJ/mol) and for guanosine (**9**) (1.3 kJ/mol), where the tunability of a purine N-nucleoside is ~ 6 times more than a C-nucleoside.

(ii) In contrast, the $\Delta\Delta G^{298}{}_{(P\text{-}N)}$ is 1.9 kJ/mol for Ψ-isocytidine (**4**) and 0.4 kJ/mol for cytidine (**10**), which means that the anomeric tunability is ~5 times larger for the former. Similarily, the $\Delta\Delta G^{298}{}_{(N\text{-}D)}$ is 1.7 kJ/mol for Ψ-uridine (**5**) and 0.2 kJ/mol for uridine (**11**), which is again 8.5 times larger for a pyrimidine C-nucleoside compared to an isosteric N-nucleoside.

(e) The comparison of the $N \rightleftarrows S$ equilibrium in purine and pyrimidine C-nucleosides

Purine C-nucleosides [79% S for (**1**), 80% S for (**2**) and 88% S for (**3**)] have more preference for S-type conformation compared to pyrimidine counterparts [63% S for (**4**), 57% S for (**5**) and (**6**), and 53% S for (**7**)], which is very similar to the situation in N-nucleosides [67% S for adenosine (**8**), 65% S for guanosine (**9**), 35% S for cytidine (**10**) and 47% for uridine (**11**)]. Thus the comparison of the magnitude of counteracting ΔH° and ΔS° contribution to ΔG° in C- or N-purine nucleosides *versus* pyrimidine counterparts gives the relative balance of N $\rightleftarrows$ S equilibrium. A perusal of values of ΔH° and ΔS° values in Table 1 show that more negative ΔH° and ΔS° values mean a shift of N $\rightleftarrows$ S equilibrium to more S-type as a result of weaker anomeric effect as found in purine C- and N-nucleosides. Table 1 also shows that a more positive ΔH° and ΔS° shift the N $\rightleftarrows$ S equilibrium to more N-type sugar as a result of stronger anomeric effect in pyrimidine C- and N-nucleosides.

(f) The energetics of the $N \rightleftarrows S$ equilibrium are different for each purine C-nucleoside

(i) The ΔG^{298} driving the N $\rightleftarrows$ S equilibrium in purine C-nucleosides both in the neutral and in the protonated state are in the following order: formycin B (**1**) (ΔG^{298}_{N} = -3.3 kJ/mol; ΔG^{298}_{P} = -1.3 kJ/mol) ≈ formycin A (**2**) (ΔG^{298}_{N} = -3.4 kJ/mol; ΔG^{298}_{P} = -2.0 kJ/mol) < 9-deazaadenosine (**3**) (ΔG^{298}_{N} = -5.0 kJ/mol; ΔG^{298}_{P} = -3.6 kJ/mol).

(ii) A comparison of pK_a between formycin A (**2**) (pK_a 4.4) and 9-deazaadenosine (**3**) (pK_a 5.9) reveal that the fused pyrazolo ring in the former has more deactivating influence on the constituent pyrimidine ring than the fused pyrrole ring in the latter. This means that the pyrazolo ring in formycin A (**2**) is more electron-deficient than the pyrrole in 9-deazaadenosine (**3**). This is the reason why the anomeric effect is stronger both in the neutral and protonated formycin A (**2**) than in 9-deazaadenosine (**3**). A similar structural comparison between neutral formycin B (**1**) (pK_a 1.4) and formycin A (**2**) (pK_a 4.4) shows why the former is less basic than the latter. This is due to the electron-withdrawing amide function in the pyrimidine part in formycin B (**1**) compared with the electron-donating amidine function in formycin A (**2**). This structural difference between these two formycin analogs in the fused pyrimidine part does not result in a different electron-deficient character of the constituent pyrazole moiety, hence their anomeric effect at the neutral state is very comparable as evident by their comparable ΔG° value (ΔG^{298}_{N} = -3.3 kJ/mol and -3.4 kJ/mol, respectively). The stabilization of their N_3H^+ form is however quite different: In the protonated formycin A (**2**), the N_3H^+ charge is stabilized by the delocalization through the amidine moiety. In the formycin B (**1**), on the other hand, the positive charge at N3 is relatively more localized which makes the constituent pyrazole ring relatively more electron-deficient than that of formycin A (**2**). Hence the anomeric drive of the N ⇄ S equilibrium is stronger in formycin B (ΔG^{298}_{P} = -1.3 kJ/mol) (**1**) than in formycin A (**2**) (ΔG^{298}_{P} = -2.0 kJ/mol).

(g) The energetics of the N ⇄ S equilibrium are different for each pyrimidine C-nucleoside

(i) The effect of the change of C1' aglycone in C-nucleosides is most clearly observed in the pyrimidine analogs compared to the purine counterparts. This is evident from the comparison of the structural characteristics of the pyrimidine moiety in formycin B (**1**) and formycin A (**2**), in one hand, and Ψ-isocytidine (**4**) and Ψ-uridine (**5**), on the other: The amide function in formycin B (**1**) and Ψ-uridine (**5**) is the same, which is simply substituted by the amidine function giving formycin A (**2**) and Ψ-isocytidine (**4**), respectively. A comparison of their ΔG^{298}_{N} shows that they are almost the same for formycin B (**1**) and formycin A (**2**) (-3.3 kJ/mol and -3.4 kJ/mol, respectively), whereas the ΔG^{298}_{N} for Ψ-uridine (**5**) and Ψ-isocytidine (**4**) are -0.6 kJ/mol and -1.4 kJ/mol, respectively. This shows that the transmission of the

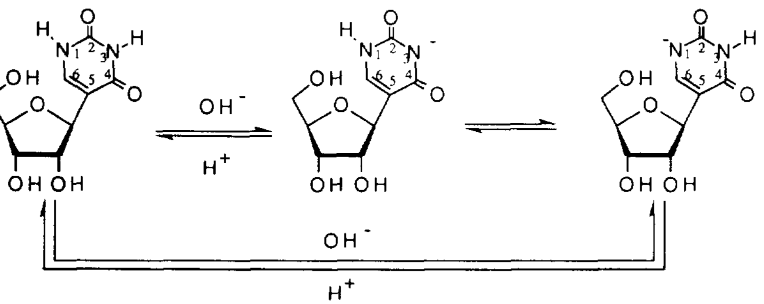

Scheme 2

electronic changes from the pyrimidine part of the purine C-nucleoside to drive the sugar conformation is poorer than the transmission from the directly connected pyrimidine aglycone, which also is the reason why small changes in the electronic character of the pyrimidine moiety in pyrimidine C-nucleosides are easily reflected by ΔG^{298} of the dynamic N ⇄ S equilibrium.

(ii) A comparison of ΔG^{298}_{N} and ΔG^{298}_{D} of Ψ-isocytidine (**4**) (ΔG^{298}_{N} = -1.4 kJ/mol; ΔG^{298}_{D} = -3.0 kJ/mol) and Ψ-uridine (**5**) (ΔG^{298}_{N} = -0.6 kJ/mol; ΔG^{298}_{D} = -2.3 kJ/mol), both in their neutral and deprotonated forms, shows that the pyrimidine aglycone in the former is more pseudoequatorial than in the latter. This is because the pyrimidine moiety in Ψ-isocytidine (**4**) is more electron-rich in both neutral and protonated forms compared to the counterparts in Ψ-uridine (**5**), hence the anomeric effect driven N $\rightleftarrows$ S equilibrium to N-form is weaker in the former than in the latter.

(iii) The anomeric drive of N $\rightleftarrows$ S equilibrium of the neutral Ψ-uridine (**5**) and 1-methyl-Ψ-uridine (**6**) is comparable (ΔG^{298}_{N} = -0.6 kJ/mol and -0.7 kJ/mol, respectively), but their anionic forms drive the sugar conformation in a considerably different manner. This is because of the larger delocalization of N1 or/and N3 negative charge(s) over the whole ring in deprotonated Ψ-uridine (**5**) (Scheme 2), thereby enhancing the negative charge at C1'. This pushes the aglycone of Ψ-uridine (**5**) into more pseudoequatorial form than that of 1-methyl-Ψ-uridine (**6**). The net result of this is a reduction of the strength of the anomeric effect in Ψ-uridine (**6**) compared to 1-methyl-Ψ-uridine (**6**).

(h) The energetics of the drive of N $\rightleftarrows$ S equilibrium are weaker in C-nucleosides than in N-nucleosides

A simple comparison of ΔG^{298}_{N}, ΔG^{298}_{P} or ΔG^{298}_{D} values of all C-nucleosides **1** - **7** (Table 1) with N-nucleosides shows that the C1' substituent promoted anomeric drive of N $\rightleftarrows$ S equilibrium to N-sugar is weaker in C- than in N-nucleosides, but their respective flexibilities from the neutral to the protonated or to the deprotonated state is completely aglycone-dependent [see section (II)(d)].

(III) The quantitation of the anomeric effect in C-nucleosides

The anomeric effect (*i.e.* ΔH° term) of C-aglycones on the drive of the two-state N$\rightleftarrows$S pseudorotational equilibrium in C-nucleosides consists of two counteracting contributions from (i) the stereoelectronic n(O4') → σ^*C1'-C(sp2) interactions between O4' lonepair and the σ^* of C1'-C(sp^2) fragment orbital in the gauche-gauche conformation, which place the aglycone in the pseudoaxial orientation, and (ii) the inherent steric effect of the nucleobase, which opposes the stereoelectronic component of the anomeric effect by its tendency to take up the pseudoequatorial orientation. The actual strength of the anomeric effect that promotes the drive of N $\rightleftarrows$ S equilibrium can be however obtained in a quantitative manner by a simple subtraction of ΔH° of a specific C-nucleoside (Table 1) from the ΔH° of the N $\rightleftarrows$ S pseudorotational drive of 1-deoxy-β-D-ribopentofuranose (**12**) (ΔH° = 0.4 kJ/mol)[1a].

(i) Thus, the strengths of the anomeric effects of neutral C-nucleosides are as follows: formycin B (**1**) (-8.5 kJ/mol), formycin A (**2**) (-8.5 kJ/mol), 9-deazaadenosine (**3**) (-14.6 kJ/mol), Ψ-isocytidine (**4**) (-2.3 kJ/mol), Ψ-uridine (**5**) (0.3 kJ/mol), 1-methyl-Ψ-uridine (**6**) (1.2 kJ/mol) and 1,3-dimethyl-Ψ-uridine (**7**) (1.6 kJ/mol).

(ii) In the acidic pD, the strengths of the anomeric effects of the protonated C-nucleosides are as follows: formycin B (**1**) (-0.9 kJ/mol), formycin A (**2**) (-2.8 kJ/mol), 9-deazaadenosine (**3**) (-7.8 kJ/mol), Ψ-isocytidine (**4**) (3.8 kJ/mol).

(iii) In the alkaline pD, the strengths of the anomeric effects of the deprotonated C-nucleosides are as follows: formycin B (**1**) (-9.2 kJ/mol), formycin A (**2**) (-8.5 kJ/mol), Ψ-isocytidine (**4**) (-8.3 kJ/mol), Ψ-uridine (**5**) (-4.9 kJ/mol) and 1-methyl-Ψ-uridine (**6**) (-3.4 kJ/mol).

From the above observations, the following can be concluded about the nature of the pD-tunable strength of the anomeric effect: (a) The strength of the anomeric effect of the C-nucleosides is tunable depending upon whether they are in the neutral, protonated or the deprotonated state. (b) The stereoelectronic component of the anomeric effect in purine C-nucleosides (**1** - **3**) is relatively small compared to the steric component in the neutral and in the deprotonated states. (c) In protonated purine-C-nucleosides, the stereoelectronic effect becomes stronger than in the neutral state but it is still overriden by the steric component. (d) In pyrimidines (**5** - **7**), the stereoelectronic component becomes stronger than the steric counterpart in the neutral state, whereas in the deprotonated pyrimidines (**4** - **6**), the stereoelectronic effect is decreasing and it is overriden by the steric effect. (e) In protonated Ψ-isocytidine (**4**), the stereoelectronic component overrides the steric component and mainly contributes to the anomeric effect.

(IV) Determination of the pK_a from the pD-dependent thermodynamics of the two-state N $\rightleftarrows$ S pseudorotational equilibrium in C-nucleosides

The plot of ΔG^{298} values (Tables 6-12) for the N $\rightleftarrows$ S pseudorotational equilibrium as a function of pD displays a sigmoidal dependence characteristic of a typical titration curve for all C-nucleosides, except for **7** (Figs. 1-7). The curves through the experimental points were fitted with the use of non-linear least-squares fitting procedure to the Henderson-Hasselbach equation: $pD = pK_a + \log(1\text{-}\alpha/\alpha)$, where α representing the fraction of protonated species[15] was calculated from the change in ΔG^{298} relative to the reference neutral state at a given pD, *i.e.* $\Delta\Delta G^{298}$, divided by the total change in their respective values between the neutral and the protonated or the deprotonated state ($\Delta\Delta G^{298}_{tot}$) This equation can then be rewrittten into the Hill equation as $pD = pK_a + \log((\Delta\Delta G^{298}_{tot} - \Delta\Delta G^{298})/\Delta\Delta G^{298})$. The pK_a values for **1** - **6** were thus determined through Hill plots of pD *versus* the logarithm of $((\Delta\Delta G^{298}_{tot} - \Delta\Delta G^{298}) / \Delta\Delta G^{298})$. Linear regression has given straight lines with Pearson's correlation coefficients (R) above 0.96 and the slopes close to one, which is a characteristic indication for the protonation involving a single protonation site, and pK_a values were obtained at the intercepts (Figs. 1-6; Table 1 and see experimental section). For formycin B (**1**), R = 0.868. This is because of the error involved in the measurement of a very small variation of temperature-dependent $^3J_{HH}$ which gives a very small change in ΔG^{298} with variation of pD throughout the alkaline pD range. The plots of counteracting ΔH° and $-T\Delta S^\circ$ that contribute to ΔG^{298} are also shown as a function of pD, and they also show sigmoidal curves giving same pK_as at the inflection points as the sigmoidal plots obtained from ΔG^{298} (Figs 1-6)

The pK_a values in **1** - **6** were also independently determined in a conventional manner by monitoring the ^{1}H-NMR chemical shifts of the non-exchangeable aromatic and anomeric protons as a function of pD of the solution at 298 K (Figs 1-6 and Table 1). The corresponding Hill plots are presented in Figs. 1- 6, and the values of α are now calculated from the change in chemical shift values relative to the reference neutral state at a given pD, divided by the total change in their respective values between the neutral and the protonated or the deprotonated state (see experimental section). Note that the pK_a values calculated from the thermodynamic parameters of N $\rightleftarrows$ S pseudorotational equilibria in **1** - **6** and the pK_as from $\Delta\delta$ in ^{1}H-NMR resonances chemical shifts are virtually identical[11,12].

(V) The transmission of the energetics of the protonation ⇄ deprotonation equilibrium drives the pD-dependent thermodynamics of the two-state N ⇄ S pseudorotational equilibrium of the sugar in C-nucleosides through the tuning of the anomeric effect

The fact that the $\Delta G°$ of the protonation ⇄ deprotonation equilibrium also drives the N ⇄ S pseudorotational equilibria is proven by the correlation plot of $\Delta\delta(^1H)$ as a function of ΔG^{298} of N ⇄ S pseudorotational equilibria in **1 - 6**, which gives a straight line (Fig. 1 - 6). The Pearson correlation coefficient (R) for the linear relationship between $\Delta\delta(^1H)$ *versus* ΔG^{298} of N⇄ S pseudorotational equilibria in **1 - 6** in Fig. 1 -6 was found to be larger than 0.96 for all nucleosides, except for formycin B (**1**, R = 0.91) because of the smaller variation of ΔG^{298} over the basic pD range (Fig. 1 - 6). The direct correlation of protonation ⇄ deprotonation equilibrium of the aglycone with the two-state N⇄ S pseudorotational equilibrium of the sugar in various C-nucleosides found in this work prooves that the force driving the protonation ⇄ deprotonation equilibrium of the heterocycle is also transmitted through the anomeric effect to drive the two-state N ⇄ S pseudorotational equilibrium.

Conclusions

We here for the first time have quantified the influence of the pD on the strength of the anomeric effect in C-nucleosides, and shown how it modulates the intrinsic bias of the two-state N ⇄ S pseudorotational equilibrium of their sugar moieties.

(1) The structural differences, as pointed out above, between the C-nucleosides (**1 - 7**), are completely reflected in their different ΔG^{298} values for N ⇄ S pseudorotational equilibrium, which are in the following increasing order: 9-deazaadenosine (**3**) < formycin A (**2**) < formycin B (**1**) < Ψ-isocytidine(**4**) < Ψ-uridine (**5**) < 1-methyl-Ψ-uridine (**6**) < 1,3-dimethyl-Ψ-uridine (**7**).

(2) The C-nucleosides show a weaker anomeric drive of N ⇄ S equilibrium compared to the N-counterparts.

(3) The protonation (or deprotonation) of the nucleobase in C-nucleosides results in an increased (or decreased) shift of the N ⇄ S pseudorotational equilibrium towards N conformations, showing the interdependency of the change of the electronic nature of the nucleobases with the dynamic conformational characteristics of the constituent pentose sugar through the transmission of the change of the strength of the anomeric effect. We expect that various metal ions binding to various nucleobases of C-nucleosides will bring about a change of the local structure equivalent to protonation or deprotonation. The change of the local structure upon such metal ion binding will be dictated by the softness or the hardness of the metal ion, its binding site as well as by the pK_a of the nucleobase, which in turn is expected to be tuned by the local microstructure of the tRNA. The tunability of the purine C-nucleosides from the neutral to the protonated or deprotonated state is comparable with the purine N-nucleosides, but the tunabilities are considerably different for the pyrimidine series. The pyrimidine C-nucleosides are much more flexible than the pyrimidine N-nucleosides, which has a considerable implication in the structural flexibility of some tRNAs: It is known that Ψ-uridine (**5**) is present ubiquitously in tRNA, and that certain tRNAs deficient in Ψ-uridine are incapable of participating in protein synthesis[2]. This implies that Ψ-uridine is more locally vulnerable to take up different

conformations, depending upon the microstructure and environment, to have certain local changes that facilitate certain cooperative conformational changes that are globally necessary for quantitative and correct biological activity of the molecule.

(4) The shift of the N $\rightleftarrows$ S equilibrium of the pentofuranosyl moiety in C-nucleosides as a function of pD displays a sigmoidal behaviour characteristic of a titration curve. Subsequent calculation of the pD values at the inflection points of the titration curves are in accordance with pK_a values of the protonation and deprotonation of the nucleobases available in the literature[11,12], and those calculated from the pD dependent aromatic and H1' chemical shifts. The direct correlation of protonation $\rightleftarrows$ deprotonation equilibrium of the aglycone with the two state N $\rightleftarrows$ S pseudoequatorial equilibrium prooves that the force driving the protonation $\rightleftarrows$ deprotonation equilibrium is also transmitted through the anomeric effect to drive the two state N $\rightleftarrows$ S pseudoequatorial equilibrium (the energy pump).

(4) The known X-ray crystal structures of C-nucleosides[16] do not reveal any anomeric effect. We have herein provided a first irrefutable experimental evidence of the existence of the tunable anomeric effect in C-nucleosides because of the fact that the ΔG° of the protonation $\rightleftarrows$ deprotonation equilibrium of the aglycone is indeed transmittable to drive the two state N $\rightleftarrows$ S pseudoequatorial equilibrium as a result of unique nature of sp^2 hybridized C-aglycone at the C1' of the pentose sugar (the stereoelectronic $n(O4') \rightarrow \sigma^*_{C1'-C(sp2)}$ interactions).

Experimental Section

(A) ^{1}H-NMR spectroscopy

^{1}H-NMR spectra were recorded at 500 MHz (Bruker DRX 500) in D_2O solution [1 mM for all compounds, δ_{CH_3CN} = 2.00 ppm as internal reference] between 278 K and 358 K at 10 K intervals in the following pD ranges: 0.5 - 11.2 for **1** (16 pDs, see Table 2), 2.2- 11.0 for **2** (14 pDs, see Table 2), 3.2 - 11.6 for **3** (13 pDs, see Table 3), 1.7 - 11.3 for **4** (15 pDs, see Table 4), 2.5 - 11.8 for **5** (9 pDs, see Table 4), 2.5 - 12.0 for **6** (9 pD's, see Table 5), 2.5 - 12.0 for **7** (3 pD's, see Table 5). The pD values correspond to the reading on a pH meter equipped with a calomel electrode calibrated with pH 4 and 7 standard buffers in H_2O and are not corrected for the deuterium isotope effect. The pD of the samples has been adjusted by the simple addition of microliter volumes of concentrated D_2SO_4 or NaOD solutions. All spectra have been recorded using 64K data points and 32 scans. The pD-dependent accurate $^3J_{HH}$ (± 0.05 Hz) (Tables 2 - 5) were obtained through simulation and iteration using DAISY program package[17] and have been used for the pseudorotational analyses.

(B) Conformational analysis with PSEUROT

The generalized Karplus equation[14b,c] used in the PSEUROT[14,18] program links coupling constants between vicinal protons to corresponding proton-proton torsion angles. The following λ substituent parameters were used for the substituents on H-C-C-H fragments : λ(C1') = λ(C3') = λ(C4') = λ(C2') = 0.62; λ(C5') = 0.68; λ(O4') = 1.27; λ(OH) = 1.26 and λ(C-aglycone) = 0.45[14c]. The PSEUROT analyses of temperature dependent $^3J_{HH}$ (278 K - 358 K, Tables 6 -12) of the sugar moieties of **1** - **7** at different pDs were performed in either one or two steps in order to carefully examine the conformational hyperspace accessible to the N and S conformers:

(i) Ψ_m(N) and Ψ_m(S) were assumed to be identical and they were kept fixed during the PSEUROT calculations, while P_N and P_S were optimized freely. (ii) When either the N-type or the S-type conformer is preferred by more than 65%, the geometry of the minor conformer was fixed while P and Ψ_m of the major conformer were optimized freely. Typically 5-10 separate PSEUROT calculations were performed in step (i) and 10 calculations in step (ii). To incorporate the error in the coupling constants (σ = 0.05 Hz), 1000 sets of randomly varied coupling constants (gaussian distribution) were generated and analyzed with a locally modified[19] version of the PSEUROT program[14] (Tables 6-12 and their legends for specific description of the conformational spaces covered by the analyses). Typically, a total of 5000-20000 individual pseudorotational analyses were performed for each compound **1** - **7** and at each pD. Some of the results were discarded due to (i) too large difference between a J_{calc} and J_{exp} (ΔJ_{max} = 0.5 Hz), (ii) too large overall rms in J_{HH} (rms_{max} = 0.3 Hz), (iii) $P_N < -40°$ or $P_N > 40°$, (iv) $P_S < 120°$ or $P_S > 180°$, or (v) $\Psi_m < 30°$ or $\Psi_m > 45°$ (see legends of Tables 6-12). The total number of pseudorotational results that were used in the subsequent calculations of thermodynamic parameters is given in column 2 of Tables 6-12. The mole fractions from the accepted pseudorotational analyses were used to construct van't Hoff plots. The averages of the slopes and the intercepts (Tables 6-12) from the 5000-20000 van't Hoff plots were used to calculate ΔH° and ΔS° (and their errors) of the N $\rightleftarrows$ S sugar equilibrium of **1** - **7** (Tables 6 - 12).

The free-energy ΔG^{298} values were calculated in two ways: (i) By taking the sum of ΔH° and -TΔS°. The standard deviation of ΔG^{298} is derived from the standard deviations of the ΔH° and -TΔS° values by the formula $\sigma=(\sigma^2_{\Delta H} + \sigma^2_{-T\Delta S})^{1/2}$ which gives a rather high error for ΔG^{298} because of the error propagation (and amplification) by the multistep procedure. (ii) From the average of the 5000-20000 individual $\ln(x_S / (1 - x_S))$ at 298K. This we refer to as $\ln_{av}(x_S / (1 - x_S))$ with its standard deviation $[\sigma \ln_{av}(x_S / (1 - x_S))]$. The free energies at 298 K, obtained by using the formula $\Delta G^{298} = -R * 0.298 * \ln_{av}(x_S / (1 - x_S))$, are presented in the last column of Tables 6-12 with their corresponding standard deviations in parentheses. The error of ΔG^{298} is then directly calculated using the formula $\sigma_{\Delta G^{298}} = -R * 0.298 * \sigma \ln_{av}(x_S / (1 - x_S))$, which is smaller compared to the one obtained with the first method. However, the value of ΔG^{298} is not changed compared to the first appraoch.

(C) Determination of the pK_a value of the aglycone from the Hill plot

The Hill plot for the δH2 of formycin B (**1**) in the acidic solution where the total change of the chemical shift of H2 ($\Delta\delta H2_{tot}$) between the neutral (7.97ppm) and the protonated (9.05 ppm) state of 1.08 ppm is used to calculate the straight line (R = 0.975) which is characterized with the slope of 1.0 (σ = 0.2) and pK_a of 1.3 (σ = 0.1) (see Panel (E) in Fig. 1). The δH2 of formycin B (**1**) shows a very small variation of 0.02ppm with pD in the alkaline solution and can therefore not be used for the determination of pK_a (not shown). The Hill plot for ΔG° of formycin B (**1**) where the total change between the neutral and the protonated state ($\Delta\Delta G°_{tot}$) of 2.0 kJ/mol is used to calculate the straight line (R = 0.980) with the slope of 1.0 (σ = 0.1) and pK_a of 1.4 (σ = 0.1) (see Panel (C) in Fig. 1). The Hill plot for ΔG° of formycin B (**1**) where the total change between the neutral and the deprotonated state ($\Delta\Delta G°_{tot}$) of 0.3 kJ/mol is used to calculate the straight line (R = 0.868) with the slope of 0.8 (σ = 0.4) and pK_a of 9.1 (σ = 0.2) (see Panel (B) in Fig. 1).

The Hill plot for the δH2 of formycin A (**2**) where the total change ($\Delta\delta H2_{tot}$) between the neutral (δ 8.16 ppm) and the protonated (δ 8.37 ppm) state of 0.21 ppm is used to calculate the straight line (R = 0.961) which is characterized with the slope of 1.2 (σ = 0.2) and pK_a of 4.4 (σ = 0.1) (see Panel (D) in Fig. 2). The Hill plot for the δH2 of formycin A (**2**) where the total change ($\Delta\delta H2_{tot}$) between the neutral (δ 8.16 ppm) and the deprotonated (δ 7.96 ppm) state of 0.20 ppm is used to calculate the straight line (R = 0.987) which is characterized with the slope of 1.1 (σ = 0.1) and pK_a of 9.5 (σ = 0.1) (see Panel (E) in Fig. 2). The Hill plot for $\Delta G°$ of formycin A (**2**) where the total change between the neutral and the protonated state ($\Delta\Delta G°_{tot}$) of 1.4 kJ/mol is used to calculate the straight line (R = 0.985) with the slope of 1.1 (σ = 0.3) and pK_a of 4.5 (σ = 0.1) (see Panel (B in Fig. 2). Note that $\Delta G°$ of formycin A (**2**) shows no variation with pD in the alkaline solution and can therefore not be used for the determination of pK_a

The Hill plot for the δH2 of 9-deazaadenosine (**3**) where the total change ($\Delta\delta H2_{tot}$) between the neutral (δ 8.10 ppm) and the protonated state (δ 8.36 ppm) of 0.26 ppm is used to calculate the straight line (R = 0.997) which is characterized with the slope of 1.1 (σ = 0.1) and pK_a of 6.0 (σ = 0.1) (see Panel (D) in Fig. 3). The additional Hill plot (not shown) made for the δH8 of 9-deazaadenosine (**3**) resulted in an value for the pK_a = 6.0 (σ = 0.2)[For H8: δ 7.59 ppm in the neutral state, δ 7.76 ppm in the protonated state; slope = 1.1 (σ = 0.1), pKa = 6.0 (σ = 0.1), R = 0.997]. The Hill plot for $\Delta G°$ of 9-deazaadenosine (**3**) where the total change between the neutral and the protonated state ($\Delta\Delta G°_{tot}$) of 1.5 kJ/mol is used to calculate the straight line (R = 0.950) with the slope of 0.9 (σ = 0.2) and pK_a of 5.9 (σ = 0.1) (see Panel (B) in Fig. 3).

The Hill plot for the δH6 of Ψ-isocytidine (**4**) where the total change ($\Delta\delta H6_{tot}$) between the neutral (δ 8.66 ppm) and the protonated (δ 8.71 ppm) state of 0.05 ppm is used to calculate the straight line (R = 0.946) which is characterized with the slope of 1.1 (σ = 0.4) and pK_a of 3.6 (σ = 0.2) (see Panel (E) in Fig. 4). The δH6 of Ψ-isocytidine (**4**) shows a very small variation of 0.02ppm with pD in the alkaline solution and can therefore not be used for the determination of pK_a (not shown). The Hill plot for $\Delta G°$ of Ψ-isocytidine (**4**) where the total change between the neutral and the protonated state ($\Delta\Delta G°_{tot}$) of 0.9 kJ/mol is used to calculate the straight line (R = 0.998) with the slope of 1.1 (σ = 0.5) and pK_a of 3.6 (σ = 0.1) (see Panel (B) in Fig. 4). The Hill plot for $\Delta G°$ of Ψ-isocytidine (**4**) where the total change between the neutral and the deprotonated state ($\Delta\Delta G°_{tot}$) of 1.6 kJ/mol is used to calculate the straight line (R = 0.996) with the slope of 0.9 (σ = 0.4) and pK_a of 9.2 (σ = 0.1) (see Panel (C) in Fig. 4).

The Hill plot for the δH1' of Ψ-uridine (**5**) where the total change ($\Delta\delta H1'_{tot}$) between the neutral (δ 4.62 ppm) and the deprotonated state (δ 4.56 ppm) of 0.06 ppm is used to calculate the straight line (R = 0.944) which is characterized with the slope of 1.6 (σ = 0.4) and pK_a of 9.1 (σ = 0.3) (see Panel (D) in Fig. 5). In this case the chemical shift of H6 changes upfield by increasing the pD with a value of 0.03 ppm between the neutral and the deprotonated state and has not been taken to calculate the pK_a. The Hill plot for $\Delta G°$ of Ψ-uridine (**5**) where the total change between the neutral and the deprotonated state ($\Delta\Delta G°_{tot}$) of 1.7 kJ/mol is used to calculate the straight line (R = 0.970) with the slope of 0.9 (σ = 0.2) and pK_a of 9.4 (σ = 0.1) (see Panel (B) in Fig. 5).

The Hill plot for the δH6 of 1-methyl-Ψ-uridine (**6**) where the total change ($\Delta\delta H6_{tot}$) between the neutral (δ 7.69 ppm) and the protonated state (δ 7.51 ppm) of 0.18 ppm is used to calculate the straight line (R = 0.988) which is characterized with the slope of 0.9 (σ = 0.1) and pK_a of 9.7 (σ = 0.1) (see Panel (D) in Fig. 6). The Hill plot for $\Delta G°$ of 1-methyl-Ψ-uridine where the total change between the neutral and the deprotonated state ($\Delta\Delta G°_{tot}$) of 0.8 kJ/mol is used to calculate the straight line (R = 0.968) with the slope of 1.0 (σ = 0.2) and pK_a of 9.9 (σ = 0.1) (see Panel (B) in Fig. 6).

Table 2. The temperature-dependent vicinal coupling constants in formycin B (**1**) and formycin A (**2**) as a function of pD[a]

	formycin B (1)							formycin A (2)					
pD	$J_{1'2'}$		$J_{2'3'}$		$J_{3'4'}$		pD	$J_{1'2'}$		$J_{2'3'}$		$J_{3'4'}$	
	278K	358K	278K	358K	278K	358K		278K	358K	278K	358K	278K	358K
0.5[b]	6.6	6.4	5.2	5.4	4.2	4.5	2.2	6.8	6.4	5.2	5.4	4.0	4.5
0.7	6.5	6.3	5.2	5.4	4.2	4.5	2.6	6.8	6.5	5.2	5.4	4.0	4.5
1.3[b]	6.9	6.6	5.2	5.4	3.8	4.3	3.4	7.0	6.6	5.3	5.5	3.9	4.5
1.7	7.3	6.7	5.2	5.4	3.6	4.4	3.8	7.1	6.6	5.3	5.5	3.8	4.2
2.3	7.7	6.8	5.3	5.5	3.1	4.3	4.3	7.3	6.7	5.2	5.5	3.1	4.1
3.6[c]	7.7	7.1	5.3	5.4	3.1	3.9	4.8[d]	7.3	6.7	5.2	5.4	3.4	4.3
5.6	7.7	6.8	5.3	5.4	3.1	4.3	5.5[d]	7.7	6.9	5.3	5.4	3.1	4.0
7.0	7.7	6.8	5.3	5.4	3.1	4.3	6.6	7.9	6.8	5.3	5.5	3.0	4.1
7.6	7.8	6.8	5.3	5.5	3.1	4.2	7.7	7.8	6.9	5.2	5.5	3.0	4.1
8.1	7.8	6.8	5.3	5.4	3.1	4.2	8.9	7.8	6.8	5.2	5.5	3.0	4.2
8.9	7.8	6.8	5.3	5.5	3.0	4.2	9.4	7.7	6.8	5.3	5.4	3.0	4.2
9.1	7.8	6.8	5.3	5.5	3.0	4.1	9.9	7.8	6.8	5.3	5.5	3.2	4.2
9.7	7.9	6.9	5.3	5.5	2.9	4.2	10.5	7.7	6.7	5.3	5.5	3.2	4.3
10.1	7.9	6.9	5.3	5.5	2.9	4.1	11.0	7.7	6.8	5.4	5.5	3.4	4.3
10.6	7.9	6.9	5.3	5.5	2.9	4.1							
11.2	7.9	6.9	5.3	5.5	2.9	4.1							

[a] In Hz, error ± 0.1 Hz. Only $^3J_{HH}$ at the lowest and the highest temperature are tabulated, whereas they are available at several intermediate temperatures in 10 K steps. Note that the complete set of $^3J_{HH}$ between 278 and 358 K at each pD have been used in the calculation of thermodynamic quantities through pseudorotational analyses and van't Hoff plots. Tabulated coupling constants are the result of simulation and iteration procedure by DAISY program.[17] [b] $^3J_{HH}$ for formycin B (**1**) could not be determined at pD = 0.5 and 1.3 above 348 K because the signals for H2'and H3' were buried under the water signal and at [c] $^3J_{HH}$ for formycin B (**1**) pD = 3.6 above 328 K because the signals for 2', 3' and 4' were buried under the water signal. [d] $^3J_{HH}$ for formycin A (**2**) could not be determined at pD = 4.8 and 5.5 below 288 K because the signals for H1'and H2'were buried under the watersignal.

Table 3. The temperature-dependent vicinal coupling constants in 9-deazaadenosine (**3**) as a function of pD[a]

	9-deazaadenosine (3)													
pD		3.2[b]	3.8[b]	4.6[b]	5.2[c]	5.9[c,d]	6.6	7.1	7.9[d]	8.5[d]	9.6[d]	10.1[d]	11.0[d]	11.6[e]
$J_{1'2'}$	278K	7.8	7.8	7.8	7.9	8.1	8.4	8.5	8.6	8.6	8.6	8.6	8.6	8.6
	358K	7.2	7.2	7.2	7.3	7.5	7.5	7.5	7.6	7.6	7.6	7.6	7.6	7.7
$J_{2'3'}$	278K	5.3	5.3	5.3	5.3	5.3	5.2	5.2	5.2	5.2	5.2	5.2	5.2	5.2
	358K	5.5	5.5	5.5	5.5	5.5	5.5	5.5	5.5	5.5	5.5	5.5	5.5	5.4
$J_{3'4'}$	278K	2.7	2.7	2.7	2.8	2.7	2.3	2.3	2.2	2.2	2.2	2.2	2.2	2.2
	358K	3.3	3.3	3.3	3.6	3.5	3.6	3.6	3.4	3.4	3.4	3.4	3.5	3.2

[a] In Hz, error ± 0.1 Hz. Only $^3J_{HH}$ at the lowest and the highest temperature are tabulated, whereas they are available at several intermediate temperatures in 10 K steps. Note that the complete set of $^3J_{HH}$ between 278 and 358 K at each pD have been used in the calculation of thermodynamic quantities through pseudorotational analyses and van't Hoff plots. Tabulated coupling constants are the result of simulation and iteration procedure by DAISY program.[17] [b] $^3J_{HH}$ for 9-deazaadenosine (**3**) at pD = 3.2, 3.8 and 4.6 could not be determined above 328 K because the signals for H2', H3', and H4' were buried under the watersignal. [c] $^3J_{HH}$ for 9-deazaadenosine (**3**) at pD = 5.2 and 5.9 could not be determined under 288 K because the signals for H1' and H2' were buried under the watersignal. [d] $^3J_{HH}$ for 9-deazaadenosine (**3**) at pD = 5.9, 7.9, 8.5, 9.6, 10.1 and 11.0 could not be determined above 348 K because the signals for H3' and H4' were buried under the watersignal. [e] $^3J_{HH}$ for 9-deazaadenosine (**3**) at pD=11.6 could not be determined above 338 K because of its decomposition.

Table 4. The temperature-dependent vicinal coupling constants in Ψ-isocytidine (**4**) and Ψ-uridine (**5**) as a function of pD[a]

Ψ-isocytidine (**4**)

pD	$J_{1'2'}$ 278K	$J_{1'2'}$ 358K	$J_{2'3'}$ 278K	$J_{2'3'}$ 358K	$J_{3'4'}$ 278K	$J_{3'4'}$ 358K
1.7[b]	4.5	5.0	5.2	5.4	6.3	5.9
2.1[b]	4.5	5.0	5.2	5.4	6.3	5.8
2.8[b]	4.8	5.3	5.1	5.4	6.2	6.6
3.7[c]	5.4	5.7	5.2	5.5	5.5	5.3
4.2[c]	5.9	6.0	5.2	5.5	4.9	5.0
4.6	6.3	6.1	5.2	5.5	4.5	4.9
5.1	6.3	6.1	5.2	5.5	4.5	5.0
6.3	6.3	6.1	5.3	5.5	4.5	4.9
7.0	6.4	6.1	5.2	5.5	4.5	4.9
7.7	6.4	6.1	5.2	5.5	4.5	4.9
8.2	6.6	6.3	5.2	5.4	4.1	5.0
8.9	7.0	6.4	5.2	5.5	3.8	4.6
9.6[c]	7.6	6.9	5.2	5.4	3.1	4.1
10.3	7.7	6.7	5.2	5.5	3.0	4.2
11.3[c]	7.8	6.9	5.2	5.4	2.8	3.9

Ψ-uridine (**5**)

pD	$J_{1'2'}$ 278K	$J_{1'2'}$ 358K	$J_{2'3'}$ 278K	$J_{2'3'}$ 358K	$J_{3'4'}$ 278K	$J_{3'4'}$ 358K
2.5	5.5	5.6	5.2	5.5	5.5	5.4
6.9	5.5	5.6	5.2	5.4	5.4	5.4
7.5	5.5	5.7	5.3	5.5	5.4	5.3
8.3	5.7	5.7	5.2	5.5	5.2	5.3
8.9	6.3	6.1	5.3	5.5	4.6	5.0
9.7	6.7	6.4	5.2	5.6	4.0	4.7
10.5	7.2	6.6	5.3	5.6	3.6	4.5
11.3	7.3	6.6	5.3	5.6	3.5	4.4
11.8	7.3	6.6	5.3	5.6	3.5	4.4

[a] In Hz, error ± 0.1Hz. Only $^3J_{HH}$ at the lowest and the highest temperature are tabulated, whereas they are available at several intermediate temperatures in 10 K steps. Note that the complete set of $^3J_{HH}$ between 278 and 358 K at each pD have been used in the calculation of thermodynamic quantities through pseudorotational analyses and van't Hoff plots. Tabulated coupling constants are the result of simulation and iteration procedure by DAISY program.[17] [b] $^3J_{HH}$ for Ψ-isocytidine (**4**) could not be determined at pD = 1.7 to 2.8 above 338 K and at [c]pD = 3.7; 4.2; 9.6 and 11.3 above 348 K because of decomposition.

Table 5. The temperature-dependent vicinal coupling constants in 1-Methyl-Ψ-uridine (**6**) and 1,3-dimethyl-Ψ-uridine (**7**) as a function of pD[a]

1-Methyl-Ψ-uridine (**6**)

pD	$J_{1'2'}$ 278K	$J_{1'2'}$ 358K	$J_{2'3'}$ 278K	$J_{2'3'}$ 358K	$J_{3'4'}$ 278K	$J_{3'4'}$ 358K
2.5	5.5	5.8	5.2	5.5	5.4	5.3
7.2	5.5	5.8	5.2	5.5	5.4	5.3
8.3[b]	5.6	5.8	5.2	5.5	5.3	5.2
8.9[b]	5.7	5.8	5.2	5.5	5.2	5.2
9.3	5.9	5.8	5.3	5.5	4.8	5.1
9.7[b]	6.1	5.9	5.2	5.4	4.7	5.0
10.5[b]	6.4	6.1	5.1	5.4	4.3	4.8
11.4[b]	6.5	6.1	5.2	5.4	4.0	4.7
12.0	6.5	6.1	5.2	5.5	4.1	4.7

1,3-dimethyl-Ψ-uridine (**7**)

pD	$J_{1'2'}$ 278K	$J_{1'2'}$ 358K	$J_{2'3'}$ 278K	$J_{2'3'}$ 358K	$J_{3'4'}$ 278K	$J_{3'4'}$ 358K
2.5	5.1	5.5	5.3	5.5	5.8	5.6
6.7	5.1	5.5	5.3	5.5	5.8	5.6
12.0	5.1	5.5	5.3	5.5	5.8	5.6

[a] In Hz, error ± 0.1 Hz. Only $^3J_{HH}$ at the lowest and the highest temperature are tabulated, whereas they are available at several intermediate temperatures in 10 K steps. Note that the complete set of $^3J_{HH}$ between 278 and 358 K at each pD have been used in the calculation of thermodynamic quantities through pseudorotational analyses. Tabulated coupling constants are the result of simulation and iteration procedure by DAISY program.[17] [b] $^3J_{HH}$ could not be determined above 348 K because the signals for H2'and H3'were buried under the watersignal.

Table 6. Pseudorotational analyses of temperature-dependent $^{3}J_{HH}$ (from 278 to 358K)^{a} at sixteen different pDs (0.5-11.2), and determination of pD-Dependent Thermodynamics of the Two State N $\rightleftarrows$ S Equilibrium for formycin B (**1**).

pD	Total number of PSEUROT analysis*	Ψ_m constrained analyses in PSEUROT$^{b, d}$		P_N and Ψ_m(N) constrained analyses in PSEUROT$^{c, d}$		Slopes and intercepts of various van't Hoff plots from ln(X_S/X_N) vs 1000/T^{e}		Thermodynamics of N $\rightleftarrows$ S Equilibrium from van't Hoff plots^{e,f}			Thermodynamics of N $\rightleftarrows$ S Equilibrium from the average populations^{g}
		P_N	P_S	P_S	Ψ_m(S)	average slopes (σ)	average intercepts (σ)	ΔH° (σ)	-TΔS° (σ)	ΔG^{298} = (ΔH° -TΔS°)	ΔG^{298} = -0.298*Rln_{av} ($x_S/(x_N)$)
0.5	18957	-34° - 39°	123° - 147°	128° - 148°	31° - 44°	0.16 (0.06)	0.12 (0.21)	-1.3 (0.5)	-0.3 (0.5)	-1.6 (0.7)	-1.5 (0.3)
0.7	19052	-38° - 40°	121° - 149°	128° - 149°	30° - 41°	0.18 (0.04)	0.04 (0.19)	-1.5 (0.4)	-0.1 (0.5)	-1.6 (0.6)	-1.6 (0.4)
1.3	11990	-33° - 40°	125° - 145°	128° - 148°	32° - 43°	0.35 (0.05)	-0.28 (0.17)	-2.9 (0.4)	0.7 (0.4)	-2.2 (0.6)	-2.2 (0.3)
1.7	10660	-35° - 40°	129° - 144°	129° - 145°	33° - 42°	0.57 (0.04)	-0.85 (0.13)	-4.7 (0.3)	2.1 (0.3)	-2.6 (0.7)	-2.6 (0.3)
2.3	12680	-36° - 40°	128° - 143°	131° - 145°	33° - 39°	0.93 (0.07)	-1.84 (0.16)	-7.7 (0.6)	4.5 (0.4)	-3.2 (0.9)	-3.2 (0.3)
3.6	11993	-37° - 39°	128° - 145°	132° - 145°	33° - 39°	0.95 (0.09)	-1.93 (0.23)	-7.7 (0.7)	4.8 (0.6)	-3.2 (0.8)	-3.2 (0.3)
5.6	12516	-34° - 20°	128° - 137°	131° - 145°	33° - 39°	0.96 (0.07)	-1.90 (0.18)	-8.0 (0.6)	4.7 (0.5)	-3.3 (0.7)	-3.3 (0.3)
7.0	12480	-34° - 16°	127° - 136°	130° - 144°	33° - 39°	0.96 (0.07)	-1.90 (0.16)	-8.0 (0.6)	4.7 (0.4)	-3.3 (0.7)	-3.3 (0.3)
7.6	12478	-37° - 40°	128° - 143°	132° - 146°	33° - 39°	0.94 (0.07)	-1.85 (0.15)	-7.8 (0.6)	4.6 (0.4)	-3.3 (0.8)	-3.3 (0.3)
8.1	12533	-35° - 40°	128° - 143°	131° - 145°	33° - 39°	0.97 (0.07)	-1.93 (0.19)	-8.1 (0.6)	4.8 (0.4)	-3.3 (0.7)	-3.3 (0.3)
8.9	12273	-37° - 40°	128° - 144°	132° - 145°	32° - 39°	1.00 (0.07)	-1.99 (0.16)	-8.3 (0.6)	4.9 (0.4)	-3.3 (0.7)	-3.4 (0.3)
9.1	12146	-37° - 40°	129° - 143°	132° - 145°	33° - 39°	1.03 (0.07)	-2.04 (0.15)	-8.6 (0.6)	5.1 (0.4)	-3.4 (0.7)	-3.5 (0.3)
9.7	11730	-32° - 17°	130° - 138°	132° - 145°	33° - 39°	1.06 (0.07)	-2.13 (0.15)	-8.8 (0.5)	5.3 (0.4)	-3.5 (0.7)	-3.5 (0.3)
10.1	12106	-33° - 40°	129° - 143°	132° - 145°	33° - 39°	1.06 (0.07)	-2.13 (0.16)	-8.8 (0.6)	5.3 (0.4)	-3.5 (0.7)	-3.5 (0.3)
10.6	12229	-33° - 40°	130° - 143°	132° - 145°	33° - 39°	1.05 (0.07)	-2.10 (0.16)	-8.7 (0.5)	5.2 (0.4)	-3.5 (0.7)	-3.4 (0.3)
11.2	11870	-32° - 40°	130° - 143°	131° - 145°	33° - 40°	1.06 (0.07)	-2.13 (0.16)	-8.8 (0.6)	5.3 (0.4)	-3.5 (0.7)	-3.4 (0.3)

^{a} $^{3}J_{HH}$ at each of sixteen pDs at 278 and 358 K are given in Table 2. ^{b} Assuming Ψ_m (N) = Ψ_m (S), we have kept Ψ_m (N) and Ψ_m (S) fixed to identical values in the range from 31° to 44° for pD = 0.5, from 33° to 45° for pD = 0.7, from 37° to 41° for pD = 1.3, 1.7 and > 9.1 and from 38° to 42° for the pDs from 2.3 - 9.1 and surveyed the conformational hyperspace in 1° steps during several PSEUROT optimizations which resulted in different populations of N and S conformers with their distinctive P_N and P_S. ^{c} P_N of the minor N-type conformers were fixed at -40° ≤ P_N ≤ 40° in 20° steps with Ψ_m (N) being simultaneously fixed at 31°and 44° for pD = 0.5, at 33°and 44° for pD = 0.7, at 37°and 41° for pD = 1.3; 1.7 and > 9.1 and at 38°and 42° for the pDs from 2.3 to 9.1 during several PSEUROT optimizations which resulted in different populations of N and S conformers with their distinctive P_N and P_S. * For each of these PSEUROT[14,19] calculations the coupling constants were 1000 times randomized which resulted in different populations of N and S conformers with their distinctive P_N and P_S (see experimental section). ^{d} The error estimates of the PSEUROT analyses have been assessed in terms of ΔJ_{max} and r.m.s., both of which are reflecting the difference between J_{calc} and J_{exp} coupling constants. The number of successful PSEUROT analyses in column 2 are designated to those which were within the constrained values (see experimental section) as well as having a ΔJ_{max} and r.m.s. values smaller than 0.5 Hz and 0.3 Hz. ^{e} The populations of N and S pseudorotamers obtained through each of the above PSEUROT calculations at nine different temperatures, shown in column 2, are the basis for the identical number of van't Hoff plots, which in turn were used to calculate the average slope and intercept. ^{f}The average of the slopes and the intercepts derived from all van't Hoff plots at a particular pD given in the columns 7 and 8 were finally used to calculate the average ΔH°, -TΔS° (at 298K) and subsequently ΔG^{298} (kJ/mol^{-1}) of N$\rightleftarrows$ S equilibria of 1. ^{g} ΔG^{298} calculated directly from the average logarithm ln_{av} (x_S/ (1- x_S)), by using the Gibbs equation ΔG^{T} = -(RT/1000)ln_{av} (x_S/ (1- x_S))with 1- x_S = x_N , R is the gas constant and T is the temperature. The standard deviations are in parentheses.

Table 7 Pseudorotational analyses of temperature-dependent $^3J_{HH}$ (from 278 to 358K)[a] at fourteen different pDs (2.2-11.0), and determination of pD-Dependent Thermodynamics of the Two State N $\rightleftarrows$ S Equilibrium for formycin A (**2**).

pD	Total number of PSEUROT analysis*	Ψ_m constrained analyses in PSEUROT[b, d]		P_N and Ψ_m(N) constrained analyses in PSEUROT[c, d]		Slopes and intercepts of various van't Hoff plots from ln(X_S/X_N) vs 1000/T[e]		Thermodynamics of N $\rightleftarrows$ S Equilibrium from van't Hoff plots[e,f]			Thermodynamics of N $\rightleftarrows$ S Equilibrium from the average populations[g]
		P_N	P_S	P_S	Ψ_m(S)	average slopes (σ)	average intercepts (σ)	ΔH° (σ)	-TΔS° (σ)	ΔG^{298} = (ΔH° -TΔS°)	ΔG^{298} = -0.298*Rln$_{av}$ ($x_S/(x_N)$)
2.2	15607	-36° - 40°	123° - 143°	127° - 146°	32° - 43°	0.29 (0.04)	-0.19 (0.14)	-2.5 (0.3)	0.5(0.3)	-2.0 (0.5)	-2.0 (0.3)
2.6	13537	-34° - 40°	123° - 143°	127° - 145°	32° - 43°	0.30 (0.04)	-0.17 (0.14)	-2.5 (0.3)	0.4(0.4)	-2.0 (0.5)	-2.0 (0.3)
3.4	14179	-29° - 40°	126° - 143°	124° - 145°	32° - 43°	0.36 (0.04)	-0.31 (0.13)	-3.0 (0.3)	0.8(0.3)	-2.2 (0.5)	-2.2 (0.3)
3.8	12778	-30° - 40°	127° - 145°	128° - 146°	32° - 43°	0.39 (0.04)	-0.32 (0.16)	-3.3 (0.3)	0.8(0.4)	-2.5 (0.5)	-2.4 (0.3)
4.3	12508	-34° - 40°	128° - 145°	131° - 147°	32° - 40°	0.53 (0.04)	-0.66 (0.13)	-4.4 (0.3)	1.6(0.3)	-2.8 (0.5)	-2.7 (0.3)
4.8	12646	-34° - 40°	128° - 145°	131° - 147°	32° - 40°	0.71 (0.05)	-1.22 (0.14)	-5.9 (0.4)	3.0(0.3)	-2.9 (0.5)	-2.7 (0.3)
5.5	12411	-35° - 40°	129° - 145°	132° - 146°	33° - 40°	0.94 (0.06)	-1.74 (0.15)	-7.8 (0.5)	4.3(0.4)	-3.5 (0.6)	-3.2 (0.3)
6.6	12742	-34° - 40°	130° - 144°	132° - 146°	33° - 40°	1.02 (0.06)	-2.03 (0.13)	-8.5 (0.5)	5.0(0.3)	-3.5 (0.6)	-3.5 (0.3)
7.7	12378	-33° - 40°	130° - 143°	132° - 145°	33° - 40°	1.01 (0.06)	-1.98 (0.14)	-8.4 (0.5)	4.9(0.3)	-3.5 (0.6)	-3.4 (0.3)
8.9	12282	-35° - 40°	128° - 137°	132° - 145°	33° - 39°	1.03 (0.06)	-2.07 (0.14)	-8.6 (0.5)	5.1(0.3)	-3.4 (0.6)	-3.4 (0.3)
9.4	11632	-35° - 40°	128° - 142°	131° - 144°	33° - 39°	1.02 (0.07)	-2.05 (0.14)	-8.5 (0.6)	5.1(0.4)	-3.4 (0.7)	-3.3 (0.3)
9.9	12177	-36° - 40°	127° - 141°	130° - 143°	33° - 39°	0.95 (0.06)	-1.83 (0.13)	-7.9 (0.5)	4.6(0.3)	-3.3 (0.6)	-3.3 (0.3)
10.5	11499	-35° - 39°	126° - 136°	129° - 143û	33° - 39°	0.93 (0.06)	-1.81 (0.13)	-7.7 (0.5)	4.5(0.3)	-3.2 (0.6)	-3.2 (0.3)
11.0	12467	-34° - 40°	126° - 142°	129° - 142°	33° - 40°	0.85 (0.05)	-1.55 (0.13)	-7.1 (0.4)	3.8(0.3)	-3.2 (0.5)	-3.2 (0.3)

[a] $^3J_{HH}$ at each of fourteen pDs at 278 and 358 K are given in Table 2. [b] Assuming Ψ_m (N) = Ψ_m (S), we have kept Ψ_m (N) and Ψ_m (S) fixed to identical values in the range from 37° to 44° for pD = 2.2 and pD=2.6 from 35° to 40° for pD = 3.8, from 37° to 41° for pD = 3.4 to 7.7 and pD=11.0; from 38 ° to 42 ° for the pDs from 8.9 to 10.5 and surveyed the conformational hyperspace in 1° steps during several PSEUROT optimizations which resulted in different populations of N and S conformers with their distinctive P_N and P_S. [c] P_N of the minor N-type conformers were fixed at -40° ≤ P_N ≤ 40° in 20° steps with Ψ_m (N) being simultaneously fixed at 37° and 44° for pD = 0.5 and pD=2.6, at 35° and 44° for pD = 3.8, at 37° and 41° for pD = 3.4 to 7.7 at 38° and 42° for the pDs from 8.9 to 10.5 during several PSEUROT optimizations which resulted in different populations of N and S conformers with their distinctive P_S and Ψ_m(S). * For each of these PSEUROT[14,19] calculations the coupling constants were 1000 times randomized which resulted in different populations of N and S conformers with their distinctive P_N and P_S (see experimental section). [d] The error estimates of the PSEUROT analyses have been assessed in terms of ΔJ_{max} and r.m.s., both of which are reflecting the difference between J_{calc} and J_{exp} coupling constants. The number of successful PSEUROT analyses in column 2 are designated to those which were within the constrained values (see experimental section) as well as having a ΔJ_{max} and r.m.s. values smaller than 0.5 Hz and 0.3 Hz. [e] The populations of N and S pseudorotamers obtained through each of the above PSEUROT calculations at nine different temperatures, shown in column 2, are the basis for the identical number of van't Hoff plots, which in turn were used to calculate the average slope and intercept. [f] The average of the slopes and the intercepts derived from all van't Hoff plots at a particular pD given in the columns 7 and 8 were finally used to calculate the average ΔH°, -TΔS° (at 298K) and subsequently ΔG^{298} (kJ/mol^{-1}) of N $\rightleftarrows$ S equilibria of **1**. [g] ΔG^{298} calculated directly from the average logarithm ln$_{av}$ (x_S/ (1- x_S)), by using the Gibbs equation ΔG^T = -(RT/1000)ln$_{av}$ (x_S/ (1- x_S))with 1- x_S = x_N , R is the gas constant and T is the temperature. The standard deviations are in parentheses.

Table 8. Pseudorotational analyses of temperature-dependent $^3J_{HH}$ (from 278 to 358K)[a] at thirteen different pDs (3.2-11.6), and determination of pD-Dependent Thermodynamics of the Two State N ⇄ S Equilibrium for 9-deazaadenosine (3).

		Ψ_m constrained analyses in PSEUROT[b, d]		P_N and $\Psi_m(N)$ constrained analyses in PSEUROT[c, d]		Slopes and intercepts of various van't Hoff plots from $\ln(X_S/X_N)$ vs 1000/T[e]		Thermodynamics of N ⇄ S Equilibrium from van't Hoff plots[e,f]			Thermodynamics of N ⇄ S Equilibrium from the average populations[g]
pD	Total number of PSEUROT analysis*	P_N	P_S	P_S	$\Psi_m(S)$	average slopes (σ)	average intercepts (σ)	ΔH° (σ)	-TΔS° (σ)	ΔG^{298} = (ΔH° -TΔS°)	ΔG^{298} = $-0.298{*}R\ln_{av}(x_S/(x_N))$
3.2	13897	-40° - 39°	133° - 150°	138° - 152°	31° - 37°	0.93 (0.09)	-1.70 (0.25)	-7.7 (0.8)	4.2 (0.6)	-3.6 (1.0)	-3.6 (0.3)
3.8	13043	-40° - 22°	133° - 145°	138° - 152°	31° - 36°	0.88 (0.10)	-1.51 (0.26)	-7.3 (0.8)	3.7 (0.6)	-3.6 (1.1)	-3.6 (0.4)
4.6	13446	-40° - 22°	133° - 145°	137° - 151°	31° - 37°	0.90 (0.10)	-1.54 (0.26)	-7.4 (0.8)	3.8 (0.6)	-3.6 (1.1)	-3.7 (0.4)
5.2	13766	-40° - 40°	130° - 144°	134° - 146°	32° - 38°	0.91 (0.10)	-1.41 (0.21)	-7.5 (0.8)	3.5 (0.5)	-4.1 (0.9)	-4.0 (0.4)
5.9	12723	-40° - 40°	131° - 143°	134° - 144°	33° - 38°	1.07 (0.11)	-1.83 (0.29)	-8.9 (0.9)	4.5 (0.7)	-4.4 (1.4)	-4.4 (0.4)
6.6	10826	-36° - 17°	134° - 140°	136° - 145°	34° - 38°	1.44 (0.13)	-2.92 (0.34)	-12.0 (1.1)	7.2 (0.8)	-4.7 (1.4)	-4.7 (1.4)
7.1	9276	-39° - 2°	132° - 135°	136° - 145°	34° - 37°	1.53 (0.14)	-3.08 (0.32)	-12.7 (1.1)	7.6 (0.8)	-5.1 (1.9)	-5.0 (0.3)
7.9	10937	-40° - 17°	132° - 139°	137° - 145°	34° - 38°	1.73 (0.18)	-3.71 (0.45)	-14.4 (1.5)	9.2 (1.1)	-5.2 (1.8)	-5.1 (0.4)
8.5	11076	-40° - 0°	133° - 139°	136° - 145°	34° - 38°	1.73 (0.18)	-3.73 (0.44)	-14.4 (1.5)	9.2 (1.1)	-5.1 (1.8)	-5.0 (0.4)
9.6	11197	-40° - 16°	133° - 139°	136° - 145°	34° - 38°	1.71 (0.17)	-3.66 (0.43)	-14.2 (1.5)	9.1 (1.1)	-5.1 (1.8)	-5.0 (0.4)
10.1	11196	-40° - 17°	133° - 140°	136° - 145°	34° - 38°	1.72 (0.17)	-3.70 (0.43)	-14.3 (1.4)	9.1 (1.1)	-5.1 (1.8)	-5.0 (0.4)
11.0	12315	-40° - 17°	134° - 141°	137° - 146°	34° - 38°	1.78 (0.20)	-3.98 (0.56)	-14.8 (1.7)	9.9 (1.4)	-5.0 (2.2)	-4.9 (0.4)
11.6	10761	-37° - 20°	134° - 140°	137° - 145°	34° - 38°	1.61 (0.15)	-3.41 (0.40)	-13.4 (1.2)	8.5 (1.0)	-4.9 (1.6)	-4.8 (0.3)

[a] $^3J_{HH}$ at each of thirteen pDs at 278 and 358 K are given in Table 3. [b] Assuming Ψ_m (N) = Ψ_m (S), we have kept Ψ_m (N) and Ψ_m (S) fixed to identical values in the range from 34° to 39° for pD = 3.2, from 35° to 40° for pD = 3.8 and pD = 4.6, from 36° to 41° for pD = 5.2; from 37° to 41° for pD = 5.9; from 38° to 40° for the pD=6.6 and pD=11.6; from 38° to 40° for pD = 6.6 and from 38° to 42° for pD«s from 7.9 to 11.0 and surveyed the conformational hyperspace in 1°steps during several PSEUROT optimizations which resulted in different populations of N and S conformers with their distinctive P_N and P_S. [c] P_N of the minor N-type conformers were fixed at $-40° \le P_N \le 40°$ in 20° steps with Ψ_m (N) being simultaneously fixed at 34°and 39° for pD = 3.2, at 35°and 40° for pDs= 3.8 and 4.6, at 36°and 41° for pD = 5.2, at 37°and 41° for pD = 5.9, at 38°and 40° for pD = 6.6, at 40°and 42° for pD = 7.1, at 38°and 42° for the pDs from 7.9 to 11.0 during several PSEUROT optimizations which resulted in different populations of N and S conformers with their distinctive P_S and Ψ_m (S). * For each of these PSEUROT[14,19] calculations the coupling constants were 1000 times randomized which resulted in different populations of N and S conformers with their distinctive P_N and P_S (see experimental section). [d] The error estimates of the PSEUROT analyses have been assessed in terms of ΔJ_{max} and r.m.s., both of which are reflecting the difference between J_{calc} and J_{exp} coupling constants. The number of successful PSEUROT analyses in column 2 are designated to those which were within the constrained values (see experimental section) as well as having a ΔJ_{max} and r.m.s. values smaller than 0.5 Hz and 0.3 Hz. [e] The populations of N and S pseudorotamers obtained through each of the above PSEUROT calculations at nine different temperatures, shown in column 2, are the basis for the identical number of van't Hoff plots, which in turn were used to calculate the average slope and intercept. [f] The average of the slopes and the intercepts derived from all van't Hoff plots at a particular pD given in the columns 7 and 8 were finally used to calculate the average ΔH°, -TΔS° (at 298K) and subsequently ΔG^{298} (kJ/mol^{-1}) of N⇄ S equilibria of 1. [g] ΔG^{298} calculated directly from the average logarithm $\ln_{av}(x_S/(1-x_S))$, by using the Gibbs equation $\Delta G^T = -(RT/1000)\ln_{av}(x_S/(1-x_S))$ with $1-x_S = x_N$, R is the gas constant and T is the temperature. The standard deviations are in parentheses.

Table 9. Pseudorotational analyses of temperature-dependent $^3J_{HH}$ (from 278 to 358K)^a at fifteen different pDs (1.7-11.3), and determination of pD-Dependent Thermodynamics of the Two State N $\rightleftarrows$ S Equilibrium for Ψ-isocytidine(**4**).

		Ψ_m constrained analyses in PSEUROT^{b,d}		Slopes and intercepts of various van't Hoff plots from $\ln(X_S/X_N)$ vs $1000/T^e$		Thermodynamics of N $\rightleftarrows$ S Equilibrium from van't Hoff plots^{e,f}			Thermodynamics of N $\rightleftarrows$ S Equilibrium from the average populations^g
pD	Total number of PSEUROT analysis*	P_N	P_S	average slopes (σ)	average intercepts (σ)	ΔH° (σ)	-TΔS° (σ)	ΔG^{298} = (ΔH° -TΔS°)	ΔG^{298} = $-0.298^*R\ln_{av}(x_S/(x_N))$
1.7	5327	-2° - 31°	120° - 135°	-0.46 (0.04)	1.36 (0.13)	3.9 (0.3)	-3.4 (0.3)	0.5 (0.5)	0.5 (0.2)
2.1	5274	-2° - 31°	120° - 133°	-0.48 (0.04)	1.42 (0.13)	4.0 (0.3)	-3.5 (0.3)	0.5 (0.5)	0.4 (0.2)
2.8	5464	-7° - 32°	120° - 135°	-0.50 (0.04)	1.61 (0.13)	4.1 (0.3)	-4.0 (0.3)	0.2 (0.5)	0.2 (0.1)
3.7	7415	-19° - 34°	120° - 135°	-0.23 (0.03)	0.99 (0.12)	1.9 (0.3)	-2.5 (0.3)	-0.5 (0.4)	-0.5 (0.1)
4.2	9730	-28° - 31°	120° - 142°	0.01 (0.04)	0.37 (0.14)	-0.1 (0.3)	-0.9 (0.3)	-1.0 (0.5)	-1.0 (0.2)
4.6	9550	-35° - 39°	120° - 145°	0.22 (0.05)	-0.23 (0.20)	-1.8 (0.4)	0.6 (0.5)	-1.2 (0.6)	-1.2 (0.2)
5.1	9520	-33° - 40°	120° - 145°	0.18 (0.04)	-0.10 (0.15)	-1.5 (0.3)	0.3 (0.4)	-1.3 (0.5)	-1.2 (0.2)
6.3	8810	-33° - 40°	120° - 143°	0.23 (0.04)	-0.22 (0.15)	-1.9 (0.3)	0.5 (0.4)	-1.3 (0.5)	-1.4 (0.2)
7.0	8938	-33° - 40°	120° - 144°	0.21 (0.04)	-0.17 (0.14)	-1.8 (0.3)	0.4 (0.3)	-1.4 (0.5)	-1.4 (0.2)
7.7	10198	-34° - 40°	120° - 144°	0.19 (0.04)	-0.09 (0.15)	-1.6 (0.3)	0.2 (0.4)	-1.4 (0.5)	-1.3 (0.2)
8.2	11153	-34° - 40°	120° - 143°	0.32 (0.03)	-0.47 (0.13)	-2.7 (0.3)	1.2 (0.3)	-1.5 (0.4)	-1.5 (0.2)
8.9	7629	-38° - 40°	122° - 143°	0.51 (0.04)	-0.89 (0.11)	-4.2 (0.3)	2.2 (0.3)	-2.0 (0.4)	-2.0 (0.2)
9.6	7040	-40° - 39°	127° - 144°	0.74 (0.06)	-1.41 (0.14)	-6.2 (0.5)	3.5 (0.3)	-2.7 (0.6)	-2.6 (0.3)
10.3	5051	-40° - 13°	127° - 138°	0.90 (0.06)	-1.82 (0.13)	-7.5 (0.5)	4.5 (0.3)	-2.9 (0.6)	-2.9 (0.2)
11.3	5318	-40° - 12°	128° - 140°	0.96 (0.07)	-1.99 (0.16)	-8.0 (0.5)	4.9 (0.4)	-3.0 (0.7)	-3.0 (0.2)

^{a} $^3J_{HH}$ at each of fifteen pDs at 278 and 358 K are given in Table 4. ^{b} Assuming Ψ_m (N) = Ψ_m (S), we have kept Ψ_m (N) and Ψ_m (S) fixed to identical values in the range from 32° to 38° for the pD 's from 1.7 to 2.8, from 32° to 40° for pD = 3.7, from 32° to 42° for pD = 4.2; from 32° to 44° for the pDs 4.6 , 7.7 and 8.2; from 32° to 43° for the pDs 5.1 to 7.0; from 32° to 45° for pD = 8.9; from 37° to 45° for pD = 9.6; from 36° to 44° for pD = 10.3; from 37° to 44° for pD = 11.3 and surveyed the conformational hyperspace in 1° steps during several PSEUROT optimizations which resulted in different populations of N and S conformers with their distinctive P_N and P_S. * For each of these PSEUROT[14,19] calculations the coupling constants were 1000 times randomized which resulted in different populations of N and S conformers with their distinctive P_N and P_S (see experimental section). ^{d} The error estimates of the PSEUROT analyses have been assessed in terms of ΔJ_{max} and r.m.s., both of which are reflecting the difference between J_{calc} and J_{exp} coupling constants. The number of successful PSEUROT analyses in column 2 are designated to those which were within the constrained values (see experimental section) as well as having a ΔJ_{max} and r.m.s. values smaller than 0.5 Hz and 0.3 Hz. ^{e} The populations of N and S pseudorotamers obtained through each of the above PSEUROT calculations at nine different temperatures, shown in column 2, are the basis for the identical number of van't Hoff plots, which in turn were used to calculate the average slope and intercept. ^{f}The average of the slopes and the intercepts derived from all van't Hoff plots at a particular pD given in the columns 7 and 8 were finally used to calculate the average ΔH°, -TΔS° (at 298K) and subsequently ΔG^{298} (kJ/mol^{-1}) of N $\rightleftarrows$ S equilibria of **1**. ^{g} ΔG^{298} calculated directly from the average logarithm $\ln_{av}(x_S/(1-x_S))$, by using the Gibbs equation $\Delta G^T = -(RT/1000)\ln_{av}(x_S/(1-x_S))$ with $1-x_S = x_N$, R is the gas constant and T is the temperature. The standard deviations are in parentheses.

Table 10. Pseudorotational analyses of temperature-dependent $^3J_{HH}$ (from 278 to 358K)[a] at nine different pDs (2.5-11.8), and determination of pD-Dependent Thermodynamics of the Two State N $\rightleftarrows$ S Equilibrium for Ψ-uridine (**5**).

pD	Total number of PSEUROT analysis*	Ψ_m constrained analyses in PSEUROT[b, d] P_N	P_S	Slopes and intercepts of various van't Hoff plots from $\ln(X_S/X_N)$ vs 1000/T[e] average slopes (σ)	average intercepts (σ)	Thermodynamics of N $\rightleftarrows$ S Equilibrium from van't Hoff plots[e,f] ΔH° (σ)	-TΔS° (σ)	ΔG^{298} = (ΔH° -TΔS°)	Thermodynamics of N $\rightleftarrows$ S Equilibrium from the average populations[g] $\Delta G^{298} = -0.298 \cdot R\ln_{av}(x_S/(x_N))$
2.5	6652	-14° - 31°	120° - 133°	-0.10 (0.03)	0.59 (0.11)	0.8 (0.2)	-1.5 (0.3)	-0.6 (0.4)	-0.6 (0.1)
6.9	6571	-17° - 30°	120° - 133°	-0.07 (0.03)	0.49 (0.12)	0.6 (0.2)	-1.2 (0.3)	-0.6 (0.4)	-0.7 (0.1)
7.5	7141	-17° - 30°	120° - 133°	-0.11 (0.03)	0.65 (0.11)	0.9 (0.2)	-1.6 (0.3)	-0.7 (0.4)	-0.7 (0.1)
8.3	7733	-20° - 39°	120° - 141°	-0.02 (0.03)	0.33 (0.13)	0.1 (0.2)	-0.8 (0.3)	-0.7 (0.4)	-0.7 (0.2)
8.9	10979	-32° - 40°	120° - 144°	0.14 (0.04)	0.03 (0.16)	-1.2 (0.3)	-0.1 (0.4)	-1.3 (0.5)	-1.2 (0.2)
9.7	6579	-38° - 40°	121° - 142°	0.31 (0.04)	-0.34(0.10)	-2.6 (0.3)	0.8 (0.2)	-1.8 (0.4)	-1.8 (0.2)
10.5	6710	-40° - 16°	123° - 135°	0.49 (0.05)	-0.73(0.11)	-4.0 (0.4)	1.8 (0.3)	-2.2 (0.5)	-2.2 (0.2)
11.3	5632	-40° - 16°	123° - 136°	0.55 (0.05)	-0.92 (0.12)	-4.6 (0.4)	2.3 (0.3)	-2.3 (0.5)	-2.3 (0.2)
11.8	5714	-40° - 15°	122° - 135°	0.57 (0.05)	-0.97 (0.11)	-4.8 (0.4)	2.4 (0.3)	-2.4 (0.5)	-2.4 (0.2)

[a] $^3J_{HH}$ at each of nine pDs at 278 and 358 K are given in Table 4. [b] Assuming Ψ_m (N) = Ψ_m (S), we have kept Ψ_m (N) and Ψ_m (S) fixed to identical values in the range from 32° to 39° for the pDs from 2.5 to 6.9, from 31° to 40° for pD = 8.3, from 31° to 43° for pD = 8.9; from 37° to 45° for the pDs 9.7, 10.5 and 11.8; from 36° to 45° for pD = 11.3; and surveyed the conformational hyperspace in 1° steps during several PSEUROT optimizations which resulted in different populations of N and S conformers with their distinctive P_N and P_S. * For each of these PSEUROT[14,19] calculations the coupling constants were 1000 times randomized which resulted in different populations of N and S conformers with their distinctive P_N and P_S (see experimental section). [d] The error estimates of the PSEUROT analyses have been assessed in terms of ΔJ_{max} and r.m.s., both of which are reflecting the difference between J_{calc} and J_{exp} coupling constants. The number of successful PSEUROT analyses in column 2 are designated to those which were within the constrained values (see experimental section) as well as having a ΔJ_{max} and r.m.s. values smaller than 0.5 Hz and 0.3 Hz. [e] The populations of N and S pseudorotamers obtained through each of the above PSEUROT calculations at nine different temperatures, shown in column 2, are the basis for the identical number of van't Hoff plots, which in turn were used to calculate the average slope and intercept. [f] The average of the slopes and the intercepts derived from all van't Hoff plots at a particular pD given in the columns 7 and 8 were finally used to calculate the average ΔH°, -TΔS° (at 298K) and subsequently ΔG^{298} (kJ/mol^{-1}) of N $\rightleftarrows$ S equilibria of **1**. [g] ΔG^{298} calculated directly from the average logarithm $\ln_{av}(x_S/(1-x_S))$, by using the Gibbs equation $\Delta G^T = -(RT/1000)\ln_{av}(x_S/(1-x_S))$ with $1-x_S = x_N$, R is the gas constant and T is the temperature. The standard deviations are in parentheses.

Table 11. Pseudorotational analyses of temperature-dependent $^3J_{HH}$ (from 278 to 358K)[a] at nine different pDs (2.5-12.0), and determination of pD-Dependent Thermodynamics of the Two State N $\rightleftarrows$ S Equilibrium for 1-Methyl-Ψ-uridine (**6**).

pD	Total number of PSEUROT analysis*	Ψ_m constrained analyses in PSEUROT[b, d]		Slopes and intercepts of various van't Hoff plots from $\ln(X_S/X_N)$ vs 1000/T[e]		Thermodynamics of N $\rightleftarrows$ S Equilibrium from van't Hoff plots[e,f]			Thermodynamics of N $\rightleftarrows$ S Equilibrium from the average populations[g]
		P_N	P_S	average slopes (σ)	average intercepts (σ)	ΔH° (σ)	-TΔS° (σ)	ΔG^{298} = (ΔH° -TΔS°)	ΔG^{298} = $-0.298*R\ln_{av}(x_S/(x_N))$
2.5	6844	-18° - 39°	120° - 140°	-0.13 (0.04)	0.73 (0.12)	1.1 (0.2)	-1.8 (0.3)	-0.7 (0.5)	-0.7 (0.1)
7.2	6795	-18° - 39°	120° - 140°	-0.14 (0.03)	0.78 (0.13)	1.2 (0.2)	-1.9 (0.3)	-0.7 (0.4)	-0.7 (0.1)
8.3	7878	-20° - 38°	120° - 141°	-0.10 (0.03)	0.57 (0.14)	0.8 (0.2)	-1.4 (0.3)	-0.6 (0.4)	-0.6 (0.1)
8.9	8330	-22° - 34°	120° - 139°	-0.05 (0.03)	0.47 (0.14)	0.4 0.2)	-1.1 (0.3)	-0.8 (0.4)	-0.8 (0.1)
9.3	10151	-29° - 37°	120° - 144°	0.10 (0.03)	0.03 (0.13)	-0.9 (0.3)	-0.1 (0.3)	-0.9 (0.4)	-1.0 (0.1)
9.7	10182	-32° - 40°	120° - 147°	0.18 (0.03)	-0.20 (0.17)	-1.5 (0.3)	0.5 (0.4)	-1.0 (0.5)	-1.0 (0.2)
10.5	9877	-34° - 40°	122° - 148°	0.29 (0.04)	-0.45 (0.14)	-2.4 (0.4)	1.1 (0.4)	-1.3 (0.5)	-1.3 (0.2)
11.4	8149	-34° - 40°	122° - 148°	0.38 (0.06)	-0.69 (0.18)	-3.1 (0.4)	1.7 (0.4)	-1.4 (0.7)	-1.4 (0.2)
12.0	8676	-34° - 40°	122° - 148°	0.35 (0.04)	-0.57 (0.15)	-2.9 (0.4)	1.4 (0.3)	-1.5 (0.5)	-1.5 (0.2)

[a] $^3J_{HH}$ at each of nine pDs at 278 and 358 K are given in Table 5. [b] Assuming Ψ_m (N) = Ψ_m (S), we have kept Ψ_m (N) and Ψ_m (S) fixed to identical values in the range from 31° to 41° for the pDs 2.5 and 7.2, from 31° to 40° for the pDs = 8.3 and 8.9; from 31° to 42° for pD = 9.3; from 31° to 43° for the pD = 9.7; from 31° to 44° for the pDs from 10.5 to 12.0 and surveyed the conformational hyperspace in 1° steps during several PSEUROT optimizations which resulted in different populations of N and S conformers with their distinctive P_N and P_S. * For each of these PSEUROT[14,19] calculations the coupling constants were 1000 times randomized which resulted in different populations of N and S conformers with their distinctive P_N and P_S (see experimental section). [d] The error estimates of the PSEUROT analyses have been assessed in terms of ΔJ_{max} and r.m.s., both of which are reflecting the difference between J_{calc} and J_{exp} coupling constants. The number of successful PSEUROT analyses in column 2 are designated to those which were within the constrained values (see experimental section) as well as having a ΔJ_{max} and r.m.s. values smaller than 0.5 Hz and 0.3 Hz. [e] The populations of N and S pseudorotamers obtained through each of the above PSEUROT calculations at nine different temperatures, shown in column 2, are the basis for the identical number of van't Hoff plots, which in turn were used to calculate the average slope and intercept. [f] The average of the slopes and the intercepts derived from all van't Hoff plots at a particular pD given in the columns 7 and 8 were finally used to calculate the average ΔH°, -TΔS° (at 298K) and subsequently ΔG^{298} (kJ/mol^{-1}) of N $\rightleftarrows$ S equilibria of **1**. [g] ΔG^{298} calculated directly from the average logarithm $\ln_{av}(x_S/(1-x_S))$, by using the Gibbs equation $\Delta G^T = -(RT/1000)\ln_{av}(x_S/(1-x_S))$ with $1-x_S = x_N$, R is the gas constant and T is the temperature. The standard deviations are in parentheses.

Table 12. Pseudorotational analyses of temperature-dependent $^3J_{HH}$ (from 278 to 358K)[a] at three different pDs (2.5-12.0), and determination of pD-Dependent Thermodynamics of the Two State N $\rightleftarrows$ S Equilibrium for 1,3-dimethyl-Ψ-uridine (7).

pD	Total number of PSEUROT analysis*	Ψ_m constrained analyses in PSEUROT[b, d]		Slopes and intercepts of various van't Hoff plots from ln(X_S/X_N) vs 1000/T[e]		Thermodynamics of N $\rightleftarrows$ S Equilibrium from van't Hoff plots[e,f]			Thermodynamics of N $\rightleftarrows$ S Equilibrium from the average populations[g]
		P_N	P_S	average slopes (σ)	average intercepts (σ)	$\Delta H°$ (σ)	$-T\Delta S°$ (σ)	ΔG^{298} = ($\Delta H°$ $-T\Delta S°$)	ΔG^{298} = $-0.298*R\ln_{av}(x_S/(x_N))$
2.5	5962	-6° - 32°	120° - 132°	-0.24 (0.03)	0.92 (0.11)	2.0 (0.2)	-2.3 (0.3)	-0.3 (0.4)	-0.3 (0.1)
6.7	5962	-6° - 32°	120° - 132°	-0.24 (0.03)	0.92 (0.11)	2.0 (0.2)	-2.3 (0.3)	-0.3 (0.4)	-0.3 (0.1)
12.0	5832	-6° - 32°	120° - 132°	-0.24 (0.03)	0.91 (0.11)	2.0 (0.2)	-2.3 (0.3)	-0.3 (0.4)	-0.3 (0.1)

[a] $^3J_{HH}$ at each of three pDs at 278 and 358 K are given in Table 5. [b] Assuming Ψ_m (N) = Ψ_m (S), we have kept Ψ_m (N) and Ψ_m (S) fixed to identical values in the range from 31° to 37° for the pDs from 2.5 to 12.0 and surveyed the conformational hyperspace in 1° steps during several PSEUROT optimizations which resulted in different populations of N and S conformers with their distinctive P_N and P_S. * For each of these PSEUROT[14,19] calculations the coupling constants were 1000 times randomized which resulted in different populations of N and S conformers with their distinctive P_N and P_S (see experimental section). [d] The error estimates of the PSEUROT analyses have been assessed in terms of ΔJ_{max} and r.m.s., both of which are reflecting the difference between J_{calc} and J_{exp} coupling constants. The number of successful PSEUROT analyses in column 2 are designated to those which were within the constrained values (see experimental section) as well as having a ΔJ_{max} and r.m.s. values smaller than 0.5 Hz and 0.3 Hz. [e] The populations of N and S pseudorotamers obtained through each of the above PSEUROT calculations at nine different temperatures, shown in column 2, are the basis for the identical number of van't Hoff plots, which in turn were used to calculate the average slope and intercept. [f] The average of the slopes and the intercepts derived from all van't Hoff plots at a particular pD given in the columns 7 and 8 were finally used to calculate the average $\Delta H°$, $-T\Delta S°$ (at 298K) and subsequently ΔG^{298} (kJ/mol^{-1}) of N$\rightleftarrows$ S equilibria of **1**. [g] ΔG^{298} calculated directly from the average logarithm $\ln_{av}(x_S/(1-x_S))$, by using the Gibbs equation $\Delta G^T = -(RT/1000)\ln_{av}(x_S/(1-x_S))$ with $1-x_S = x_N$, R is the gas constant and T is the temperature. The standard deviations are in parentheses.

Acknowledgements

We thank the Swedish Board for Technical Development and Swedish Natural Science Research (NFR) Council, Swedish Board for Technical Development (NUTEK), Sweden and the D. Collen Research foundation, Belgium for generous financial support. Thanks are due to the Wallenbergstiftelsen, Forskningsrådsnämnden, and University of Uppsala for funds for the purchase of 500 and 600 MHz Bruker DRX NMR spectrometers. Authors are indebted to Prof. K. A. Watanabe for generous gift of some C-nucleosides studied in this work.

References and Notes

1. (a) Plavec, J.; Tong, W.; Chattopadhyaya, J. *J. Am. Chem. Soc.* **1993**, *115*, 9734. (b) Plavec, J.; Garg, N.; Chattopadhyaya, J. *J. Chem.Soc., Chem. Commun.* **1993**, 1011. (c) Plavec, J.; Koole, L. H.; Chattopadhyaya, J. *J. Biochem. Biophys. Meth.* **1992**, *25*, 253. (d) Koole. L. H.; Buck, H. M.; Nyilas, A.; Chattopadhyaya, J. *Can J. Chem.* **1987**, *65*, 2089. (e) Koole, L. H.; Buck, H. M.; Bazin, H.; Chattopadhyaya, J. *Tetrahedron* **1987**, *43*, 2289. (f) Koole, L. H.; Plavec, J.; Liu, H.; Vincent, B. R.; Dyson, M. R.; Coe, P. L.; Walker, R. T.; Hardy, G. W.; Rahim, S. G.; Chattopadhyaya J. *J. Am. Chem. Soc.* **1992**, *114*, 9934. (g) Plavec, J.; Thibaudeau, C.; Viswanadham, G.; Sund, C.; Chattopadhyaya, J. *J. Chem. Soc., Chem. Comm.* **1994**, 781. (h) Thibaudeau, C.; Plavec, J.; Watanabe, K. A.; Chattopadhyaya, J. *J. Chem. Soc., Chem. Comm.* **1994**, 537. (i) Thibaudeau, C.; Plavec, J.; Garg, N.; Papchikhin, A.; Chattopadhyaya, J. *J. Am. Chem. Soc.* **1994**, *116*, 4038. (j) Plavec, J.; Thibaudeau, C.; Chattopadhyaya, J. *J. Am. Chem. Soc.* **1994**, *116*, 6558. (k) Thibaudeau, C.; Plavec, J.; Chattopadhyaya, J. *J. Am. Chem. Soc.* **1994**, *116*, 8033. (l) J. Plavec Ph.D. Thesis, Department of Bioorganic Chemistry, Uppsala University, Sweden, **1995**. (m) Plavec, J.; Thibaudeau, C; Chattopadhyaya, J. *Tetrahedron* **1995**, *51*, 11775. (n) Thibaudeau, C. ; Plavec, J. and Chattopadhyaya, J. *J. Org. Chem.* **1996**, *61*, 266. (o) Chattopadhyaya, J. *Nucl. Acids Symposium Series* **1996**, *35*, 111. (p) Plavec, J.; Thibaudeau, C. and Chattopadhyaya, J. *Pure and Applied Chemistry,* **1996**, 68, 2137. (q) Thibaudeau, C. and Chattopadhyaya, J. *Nucleosides & Nucleotides* **1997**, in press. (r) Thibaudeau, C. and Chattopadhyaya, J. *J. Org. Chem.*, **1996**, submitted.
2. (a) Cortese, R.; Kammen, H. O.; Spengler, S. J. and Ames, B. N. *J. Biol. Chem.* **1974**, *249*, 1103. (b) Samuelsson, T.; Boren. T.; Johansen, T. I. and Lustig, F. *J. Biol. Chem.* **1988**, *263*, 13692.
3. (a) Suhadolnik, R. J. *Nucleoside Antibiotics,* Wiley-Interscience, New York **1970**; *Nucleosides as Biochemical Probes,* Wiley-Interscience, New York **1979**; Townsened L. B. in *Handbook of Biochemistry and Molecular Biology,* 3rd ed., (Fasman G. D. ed.), *Vol. 1,* p 271, CRC Press, Columbus, Ohio **1975** (b) Hanessian, S. and Pernet, A. G. *Adv. Carbohydr. Chem. Biochem.* **1976**, *33*, 111. (c) Daves, G. D. and Cheng, C. C. *Prog. Med. Chem.* **1976**, *13*, 303. (d) Buchanan J. G. *Forsch. Chem. Org. Naturst.* **1983**, *44* 243. (e) Hacksell, U. and Daves, G. D. *Prog. Med. Chem.* **1985**, *22*, 1. (f) There are other types of C-glycosyl natural products in which the aglycons are not nitrogen heterocycles. Some of these C-glycosyl compounds have shown anticancer activity. Daves G. D. *Acc. Chem. Res.* **1990**, *23*, 201.
4. (a) Tvaroska, I.; Bleha, T. *Adv. Carbohydr.Chem.* **1989**, *47*, 45. (b) Juaristi, E.; Cuevas, G. *Tetrahedron* **1992**, *48*, 5019. (c) Petillo, P. A.; Lerner, L. A. in *The Anomeric Effect and Associated Stereoelectronic Effects,* Thatcher, G. R .J. Ed., ACS Symposium Series: Washington, DC, **1993**, pp. 156. (d) Box, V. G. S. *Heterocycles* **1990**, *31*, 1157. (e) Olson, W.K.; Sussman, J.L. *J. Am. Chem. Soc.* **1982**, *104*, 270. (f) Olson, W.K. *J. Am. Chem. Soc.* **1982**, *104*, 278. (g) Phillips, L.; Wray, V. *J. Chem. Soc., Chem. Commun.* **1973**, 90. (h) Brunck, T.K.; Weinhold, F. *J. Am. Chem. Soc.* **1979**, *101*, 1700. (i) Murcko, M.A.; DiPaola, R.A. *J. Am. Chem. Soc.* **1992**, *114*, 10010. (j) Wiberg, K.B.; Murcko, M.A.; Laidig, K.E.; MacDougall, P.J. *J. Phys. Chem.* **1990**, *94*, 6956.
5. Edward, J.T. *Chem. Ind. (London)* **1955**, 1102.
6. (a) Lucken, E. A. C.*J. Chem. Soc.* **1959**, 2954. (b) Romers, C.; Altona, C; Buys, H. R.; Havinga, E. *Top. Stereochem.* **1969**, 4, 39.
7. Saenger, W. *Principles of Nucleic Acid Structure,* Springer Verlag, Berlin, **1988** .
8. Perrin, C. L.; Armstrong, K. B.; Fabian, M. A. *J. Am. Chem. Soc.* **1994**, *116*, 715.
9. Salzner, U. *J. Org. Chem.* **1995**, *60*, 986.
10. Cosse-Barbi, A.; Watson, D. G.; Dubois, J.E. *Tetrahedron Lett.* **1989**, *30*, 163.
11. "Dictionary of Organic Compounds", volume 3, fifth edition, Chapman and Hall, New York, and references therein.
12. Ward, D. C., Reich, E. and Stryer, L. *J. Biol. Chem.* **1969**, *244*, 1228.
13. Watanabe, K. A. *Chem. Nucleosides Nucleotides* **1994**, *3*, 421. Ed. Townsed, L.B. (Plenum; New York).

14. (a) De Leeuw, F. A. A. M. and Altona, C. *J. Comp. Chem.* **1983**, *4*, 428 and PSEUROT, QCPE program No 463. (b) Diez, E.; Fabian, J. S.; Guilleme, J.; Altona, C. and Donders, L.A. *Mol. Phys.* **1989**, *68*, 49. (c) Donders, L. A.; de Leeuw, F. A. A. M. and Altona, C. *Magn. Reson. Chem.* **1989**, *27*, 556. (d) Altona, C.; Ippel, J.H.; Hoekzema, A. J. A. W.; Erkelens, C.; Groesbeek, G.; Donders, L.A. Magn. Res. Chem. **1989**, *27*, 564. (e) Van Wijk, J., unpublished result.
15. Wyman, J. and Gill, S. J. *Binding and Linkage. Functional Chemistry of Biological Macromolecules;* University Science Books: Mill Valley, CA, **1990**, 330.
16. (a) The differences between C4'-O4' and O4'-C1' bond distances in X-ray crystal structures of most β-D-ribofuranosyl-*C*-nucleosides are smaller (≈0.01 Å) than in *N*-counterparts (≈0.03 Å) and therefore we were uncertain of the presence (ref. 1h) of the anomeric effect in β-D-ribofuranosyl-*C*-nucleosides. For the X-ray crystal structures of pyrimidine β-D-ribofuranosyl-*C*-nucleoside 4-thio-ψ-uridine, see Barnes, C.L.; Hawkinson, S.W.; Wigles, P.W. *Acta Crystallogr., Sect. B* **1980**, *36*, 2299; for isocytidine hydrochloride, see Birnbaum, G.I.; Watanabe, K.A.; Fox, J.J. *Can. J. Chem.* **1980**, *58*, 1633; for 2'-chloro-2'-deoxy-1,3-dimethyl-ψ-uridine, see Pankiewicz, K.W.; Watanabe, K.A.; Takayanagi, H.; Itoh, T.; Ogura, H. *J. Heterocycl. Chem.* **1985**, *22*, 1703. The X-ray crystal structures of some purine β-D-ribofuranosyl- *C*-nucleosides have been also elucidated by Koyama, G.; Nakamura, H.; Umezawa, H.; Iitaka, Y. *Acta Crystallogr., Sect. B* **1976**, *32*, 813 [for formycin B (**2**)], Abola, J.E.; Sims, M.J.; Abraham, D.J.; Lewis, A.F.; Townsend, L.B. *J. Med. Chem.* **1974**, *17*, 62 (for 2-methyl-formycin A), Prusiner, P.; Brennan, T.; Sundaralingam, M. *Biochemistry* **1973**, *12*, 1196 (for formycin A monohydrate).
17. DAISY, Spin Simulation Program, provided by Bruker, was used with 7 spins systems.
18. Altona, C.; Sundaralingam, M. *J. Am. Chem. Soc.* **1972**, *94*, 8205; *ibid* **1973**, *95*, 2333.
19. Our modification of the PSEUROT v.5.4 program (ref 14) is intended to make it possible to evaluate and assess the propagation of errors from the experimental J_{HH} throughout the PSEUROT calculations as well as throughout subsequent treatment of the obtained data. Our modified program has retained all features of the original PSEUROT program, all changes are additions. The estimated error, expressed as standard deviation (σ), for each J_{HH} is entered to the program as well as the desired number of sets of randomly varied J_{HH}s to be generated and subsequently analyzed by pseudorotational analyses. Typically, 1000 data sets are generated and individually analyzed. Each set of 'experimental data' will contain randomly varied J_{HH}s but over all the data sets, each J_{HH} is normally distributed around its experimental value with the given σ. The output from our modified program consists of statistical data (average, σ and skew of the calculated geometrical parameters and mole fractions as well as of the generated J_{HH}s) and results from all the individual pseudorotational analyses (the calculated geometrical parameters and mole fractions). It is also possible to discard results which fall outside given ranges (J_{calc}-J_{exp}, rms in J_{HH}, P_N, P_S, Ψ_m(N) and Ψ_m(S)).
20. proFit version 4.2, Quantum Soft, Postfach 6613, CH - 8023 Zürich, Switzerland **1990-94**

(*Received in UK* 10 *February* 1997; *revised* 17 *March* 1997; *accepted* 20 *March* 1997)